AGU ADVANCING EARTH AND SPACE SCIENCES

JGR Atmospheres

RESEARCH ARTICLE
10.1029/2025JD044431

Key Points:

- 47% of wet season rain moisture originated from land evapotranspiration, while sub-cloud evaporative loss was ~30% of total rain volume
- Stratiform rainfall events are linked to increased sub-cloud evaporative losses
- Stable isotope composition of low-volume rain events can significantly bias monthly weighted means

Supporting Information:

Supporting Information may be found in the online version of this article.

Correspondence to:

G. Skrzypek,
Grzegorz.Skrzypek@uwa.edu.au

Citation:

Wan, C., Dogramaci, S., Gleeson, J., Hedley, P., Grierson, P., Gibson, J. J., & Skrzypek, G. (2026). Stable isotope record of precipitation dynamics in the semi-arid subtropics. *Journal of Geophysical Research: Atmospheres*, *131*, e2025JD044431. https://doi.org/10.1029/2025JD044431

Received 27 MAY 2025
Accepted 1 MAR 2026

Author Contributions:

Conceptualization: Shawan Dogramaci, Pauline Grierson, Grzegorz Skrzypek
Data curation: Paul Hedley, Grzegorz Skrzypek
Formal analysis: Chengwei Wan, Grzegorz Skrzypek
Funding acquisition: Shawan Dogramaci, Grzegorz Skrzypek
Investigation: Shawan Dogramaci, Jennifer Gleeson, Paul Hedley
Methodology: Chengwei Wan, John J. Gibson
Project administration: Jennifer Gleeson, Paul Hedley, Grzegorz Skrzypek

Stable Isotope Record of Precipitation Dynamics in the Semi-Arid Subtropics

Chengwei Wan[1], Shawan Dogramaci[1,2,3], Jennifer Gleeson[4], Paul Hedley[4], Pauline Grierson[1], John J. Gibson[5], and Grzegorz Skrzypek[1]

[1]West Australian Biogeochemistry Centre, School of Biological Sciences, The University of Western Australia, Perth, WA, Australia, [2]Northern Star Resources Limited, Subiaco, WA, Australia, [3]College of Science & Engineering, Flinders University, Adelaide, SA, Australia, [4]Rio Tinto Iron Ore, Perth, WA, Australia, [5]InnoTech Alberta, Victoria, BC, Canada

Abstract Global climate change is profoundly affecting precipitation patterns worldwide, including the exacerbation of aridity in dryland regions. Here, we examined the variability in rainfall stable hydrogen and oxygen isotope compositions (δ^{18}O and δ^{2}H) at five locations in subtropical northwest Australia over 10 years (2015–2024) to better understand the mechanisms driving precipitation and to identify moisture sources. We found that precipitation with low δ^{2}H and δ^{18}O was predominantly observed during months with high rainfall, confirming the significant impact of the "amount effect" at most sites. δ^{2}H and δ^{18}O were positively correlated with the stratiform fraction of total precipitation, which indicates the importance of sub-cloud evaporation losses during stratiform events. The mean sub-cloud evaporated fraction was estimated at ~30%; a back trajectory analysis revealed that up to 47% of rain moisture during the wet season was recycled from land evapotranspiration. Differences between arithmetic and volume-weighted monthly mean stable isotope compositions highlight the seasonal significance of small-volume rainfall events for monthly means. We propose a new "cut-off" approach to eliminate the disproportionate influence of a high proportion of low-volume rainfall on the stable isotope composition of monthly precipitation and Local Meteoric Water Lines.

Plain Language Summary To better understand how rainfall forms in the semi-arid tropics, we analyzed stable hydrogen and oxygen isotope composition of rainwater collected over 10 years (2015–2024) from five locations in northwestern Australia. We found that rain had lower ratios of heavy-to-light stable isotopes in months of higher rainfall, confirming that the amount of rain, rather than air temperature, primarily influences rainwater stable isotope composition in semi-arid regions. We also discovered that rain originating from certain cloud types experiences greater sub-cloud evaporation, particularly during smaller events. On average, approximately 30% of the rainwater evaporates before reaching the ground. We also employed weather-tracking tools to trace the sources of moisture contributing to rainfall. During the wet season, up to half of the rainfall came from water recycled through the land surface and plant evaporation. We also found that small rain events, despite their low volume, can significantly impact the monthly average stable isotope composition. To address this bias, we propose a new method to reduce the impact of small rainfall events when analyzing long-term rain data.

1. Introduction

Precipitation patterns in semi-arid regions worldwide may be more profoundly impacted by climate change than in wetter areas (Lian, 2021). Increased aridity has been observed in North America, the Mediterranean, Central Asia and parts of Australia (Huang et al., 2017), while in others, the usual seasonal precipitation patterns are disrupted (Cai et al., 2012). However, climate model predictions of future rainfall changes for these regions are highly uncertain, although they generally predict an increase in the intensity and frequency of extreme precipitation events (Debeire et al., 2025). Models that might be down-scaled to regional levels are, however, also constrained by a limited understanding of local atmosphere-land coupling mechanisms and how rainfall forms under different conditions (Sekizawa et al., 2018; Sharmila & Hendon, 2020).

In the dry sub-tropics of the Pilbara region of northwest Australia, extreme spatial and temporal variability in rainfall poses a significant challenge to understanding hydrologic processes and thus the development of best practice in managing water resources and conserving environmental services. The Pilbara (an area approximately equivalent in size to Spain) is one of the world's most significant iron ore mining areas, including extensive areas that mine below the water table (Rojas et al., 2018). Mining activities occur within a landscape of significant

Resources: Shawan Dogramaci, Jennifer Gleeson, Paul Hedley, Pauline Grierson, Grzegorz Skrzypek
Supervision: Shawan Dogramaci, Jennifer Gleeson, Paul Hedley, Pauline Grierson, Grzegorz Skrzypek
Validation: Chengwei Wan, John J. Gibson, Grzegorz Skrzypek
Writing – original draft: Chengwei Wan
Writing – review & editing: Shawan Dogramaci, Pauline Grierson, John J. Gibson, Grzegorz Skrzypek

ecological and heritage values, including many springs, water holes and ephemeral wetlands that are culturally important to First Nations people.

The Pilbara region is characterized by distinct dry winter (April–October) and wet summer seasons (November–March). The region has more cyclone-driven precipitation than other parts of Australia, resulting in large seasonal and year-to-year variability (Fierro & Leslie, 2014). Cyclones can also trigger extreme but relatively short-lived flash flooding events that are separated by periods of prolonged droughts (Clark et al., 2018; Shi et al., 2008). Furthermore, the high variability of regional precipitation patterns, both within and among years, may be driven by mechanisms that remain only partially understood. The primary precipitation drivers in this region include synoptic-scale weather systems that dominate short-term patterns, while regional climate feedbacks can exert a longer-term influence. Climate drivers such as the El Niño Southern Oscillation (ENSO), the Indian Ocean Dipole (IOD) and the Madden-Julian Oscillation (MJO) influence rainfall patterns on interannual to seasonal timescales (Berry et al., 2011; Borowiak et al., 2023). Therefore, improving the understanding of precipitation dynamics associated with these different rainfall drivers would facilitate more accurate predictions of water availability, drought mitigation, and flood risk, and contribute to better water-use planning in the future (Rouillard et al., 2015).

Previous studies conducted elsewhere have demonstrated that rainfall isotope composition provides robust insights into precipitation dynamics, local meteorological and hydrological conditions, and broader perspectives on moisture sources and air parcel trajectories (Crawford et al., 2017; Munksgaard et al., 2020). Rainfall stable isotope studies have been conducted at various locations across Australia in recent decades, with most of the research focused on south eastern Australia, for example, Tasmania (Barras & Simmonds, 2008), Adelaide (Guan et al., 2013), Melbourne (Barras & Simmonds, 2008), Sydney (Crawford et al., 2023; Hughes & Crawford, 2013), as well as Cairns (Munksgaard et al., 2020) and Darwin (Zwart et al., 2016, 2018). Coastal climates influence most of these study locations. In contrast, the number of inland studies focused on areas characterized by a semi-arid climate is limited to Macquarie Marshes in northwest New South Wales (Crawford et al., 2017) and Alice Springs in central Australia (Hollins et al., 2018). There are also limited records available from the Global Network for Isotopes in Precipitation (GNIP) database. Rainfall isotope data sets are scarce for Western Australia (more than one-third of the continent); the only regions with multiannual records have been established in Perth (Hollins et al., 2018) and southwest Western Australia (Griffiths et al., 2022), where the climate is warm and wet, in stark contrast to the hot and dry conditions of the Pilbara in northwest Western Australia. To our knowledge, Skrzypek et al. (2019) is the only study to date that has reported the isotopic composition of monthly rainfall samples for the Hamersley Basin, but only over 12 months. A longer-term and detailed assessment of variation in the isotope composition of rainfall would greatly improve our understanding of rainfall patterns and implications for hydrologic processes.

The prominent correlation between stable isotope composition and rain amounts, the so-called "amount effect," is often used to characterize pantropical precipitation (Dansgaard, 1964). However, while subsequent studies of Dansgaard have reported insignificant or even reverse correlations, there is a broader consensus regarding isotope variability associated with stratiform versus convective precipitation types. In general, rainfall $\delta^{18}O$ exhibits a negative correlation with the stratiform fraction, a relationship that has gained widespread acceptance and is commonly applied in paleoclimate and hydrology studies (Aggarwal et al., 2016; Chang et al., 2020). Recent debates have explored the inherent isotope fractionation mechanisms associated with different rain types (Yu et al., 2024). A central debate has been whether or not raindrop re-evaporation and isotope exchange are more effective during small-magnitude stratiform precipitation events, resulting in more positive delta values in precipitation (Kaseke et al., 2018). Based on simulations, the latest research suggests that deep convection (stratiform fraction 0%) generally produces the lowest $\delta^{18}O$ in precipitation (Landshuter et al., 2024).

Crawford et al. (2017) recently showed that nearly 20% of raindrop volumes evaporated under a cloud base before reaching the ground surface in a study of semi-arid areas in eastern Australia. We might thus expect sub-cloud evaporation to be a significant driver in the Pilbara region (see also Wang et al., 2024). The prevalence of stratiform precipitation events in the Pilbara, however, is primarily influenced by convective systems associated with cyclones and other low-pressure systems (Sun et al., 2022). We hypothesize here that this form of precipitation may also increase the raindrop re-evaporation process, potentially masking the "amount effect" and leading to a causal misinterpretation of precipitation isotope variability in previous assessments.

Broadly, there is a significant research gap in understanding how local meteorological conditions and the history of air mass movements influence the stable isotope composition of rainfall at the ground level in semi-arid climates. Understanding the drivers of stable isotope variability in rainfall will provide insights into moisture origin and help determine whether the increasing rainfall trend observed over recent decades in the Pilbara (in contrast to the drying observed in many other arid regions) will persist and result in increased recharge, soil water storage and stream flows. Water stable isotope mass balance has been demonstrated as an effective method for estimating evaporative losses, water use by plants, and to estimate soil moisture retention and groundwater recharge (e. g., Dogramaci et al., 2012; Harrington et al., 2002; Skrzypek et al., 2019, 2023; Tugwell-Wootton et al., 2020; X. Xu et al., 2025). However, these approaches rely fundamentally on a nuanced understanding of how stable isotope compositions in rainfall vary across environmental gradients, particularly with respect to distance from the coast, elevation, and aridity (Skrzypek et al., 2023).

This study, based on a 10-year record of monthly rainfall isotopes in the Pilbara region, has targeted filling this regional gap in Australia, aiming to (a) explain the spatial and temporal variability of rainfall isotope compositions in a semi-arid climate; (b) identify the key processes controlling precipitation dynamics in semi-arid climate regions in general; and (c) to examine whether the GNIP monthly sampling scheme is appropriate for hydrologic applications in semi-arid climates.

2. Materials and Methods

2.1. Study Area

The Pilbara region of northwestern Western Australia includes the Ashburton, Onslow Coast, Fortescue, Port Hedland Coast and De Grey River Basins (Australian Water Resources Council). The climate is sub-tropical, ranging from semi-arid to arid, and with two broadly defined seasons: the dry season coincides with the austral winter (May–October) when temperatures are cool-warm and rainfall sparse, while the wet season (November–April) coincides with the austral summer, with very hot temperatures, high humidity and occasionally intense large rainfall events that are heavily influenced by tropical cyclones and low pressure systems. Average maximum daily temperatures between November and March typically exceed 35°C (Charles et al., 2013). Large-scale processes, such as the IOD, ENSO, and possibly the Southern Annular Mode (SAM) (see O'Donnell et al., 2015) are the main large-scale drivers likely influencing the frequency and intensity of rainfall.

During the 10-year study period (2015–2024), over 80% of rainfall occurred between December and March, as observed by five weather stations (Figure 1). The lowest mean annual rainfall was 288 mm in Robe River (ROBE, near the coast), while the highest mean annual rainfall was 366 mm in Gudai-Darri (KADA, formerly Koodaideri). The yearly mean relative humidity was low during the observation period, ranging between 30% and 37%, and the fluctuation between the highest and lowest monthly values was within 20%. Consequently, the potential evaporation rates were very high and could exceed 3,000 mm (McFarlane et al., 2015; Skrzypek et al., 2019). The annual average temperatures showed an increasing trend over the study period, ranging between 24.6 and 28.3°C in 2015 and rising to 26.3–27.8°C in 2023 among the five sites (Text S2 and Figure S1 in Supporting Information S1). Total annual precipitation as well as precipitation types showed significant variations (Figure S2 in Supporting Information S1); the highest precipitation ranged from 423 to 540 mm (2015), while the lowest annual precipitation ranged from 121 to 218 mm (2019) across all five sites (Figure 1 and Figure S1 in Supporting Information S1).

2.2. Monthly Rainfall Sampling and Stable Hydrogen and Oxygen Isotope Analyses and Data Quality

In accordance with GNIP/IAEA guidelines (IAEA Sampling Protocol), monthly cumulative rainwater samples (http://www-naweb.iaea.org/napc/ih/documents/userupdate/sampling.pdf.) were systematically collected using Palmex rainwater collectors (Zagreb, Croatia) featuring a 135 mm funnel diameter and a 3,000 mL high-density polyethylene (HDPE) bottle. The collectors were installed at a height of 1.0–1.5 m above ground level, following the design described by Gröning et al. (2012). The five sites in the Pilbara region selected to collect the monthly rain samples that were paired with meteorological observations are: Hope Downs 4 (HD4), Paraburdoo (PARA), Marillana (MARIL), Gudai-Darri (KADA) and Robe River (ROBE) (Figure 1).

Composite rainfall samples were collected in the collector container for at most 1 month. At the end of each month, the total volume was recorded and a subsample was transferred to a 25 mL glass vial, which was stored in a

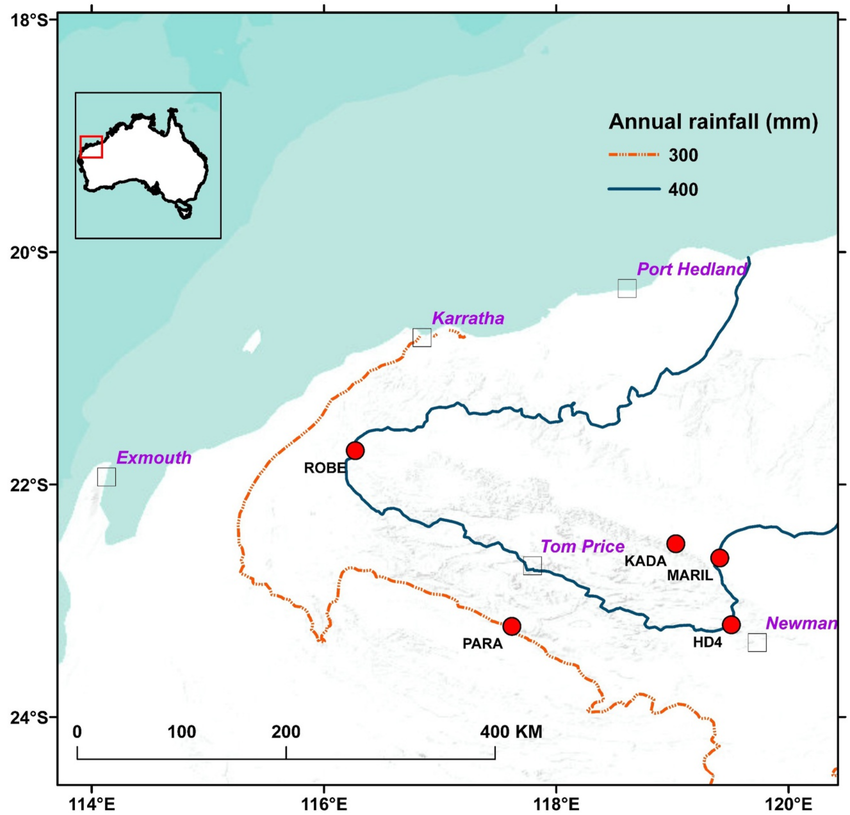

Figure 1. Locations of rainfall sampling sites in northwestern Western Australia. The dashed lines represent the mean annual rainfall calculated from the 1991–2020 data set from the Australian Bureau of Meteorology (product IDCJCM004).

fridge at 4°C. The sampling period covered the years 2015–2024, but the data set length for each site varied (Table S1 in Supporting Information S1). A total of 214 monthly rainfall samples were collected, although 13%–29% of the months were missing at each site. Notably, the uncollected months accounted for less than 20% of the total rainfall during the observation period, thereby ensuring the hydrological representativeness of the data set (details in Table S9 in Supporting Information S1). The most comprehensive data set (50 monthly samples) was obtained for HD4 collected between May 2015 and March 2024.

Rainfall samples were sent after each collection to the West Australian Biogeochemistry Center at The University of Western Australia for stable hydrogen and oxygen isotope analyses. Samples were analyzed using a Picarro L1102-I and 2130 Isotopic Liquid Water Analyzer (Picarro, Santa Clara, California, USA). Each sample was analyzed six times with the first three results discarded to minimize potential instrument memory effects and drift corrected. The raw δ^2H and δ^{18}O values of the samples were normalized to the VSMOW (Vienna Standard Mean Ocean Water) scale, based on three laboratory standards, and reported in permille (‰) following the principles of three-point normalization (Skrzypek & Ford, 2014). All laboratory standards covered the whole range of sample values and were calibrated against international reference materials that define the scale (Coplen et al., 1996) provided by the International Atomic Energy Agency (with VSMOW2 values of $\delta^2\text{H} = 0‰$ and $\delta^{18}\text{O} = 0‰$, and SLAP2 values of $\delta^2\text{H} = -428.0‰$ and $\delta^{18}\text{O} = -55.5‰$). The long-term analytical uncertainty (one standard deviation) was determined to be <1.0‰ for δ^2H and <0.1‰ for δ^{18}O (Skrzypek, 2013; Skrzypek & Ford, 2014). Deuterium excess (d-excess) was calculated as $\text{d-excess} = \delta^2\text{H} - 8 \times \delta^{18}\text{O}$ (Dansgaard, 1964).

Secondary evaporation of low-volume water samples remaining in the tube-dip-in-water collector for up to 32 days has been identified in previous studies (Michelsen et al., 2018; Natali et al., 2024). When the monthly precipitation volume was <6.3 mm, the collector inlet tube might not be submerged in water and cause evaporative isotope fractionation (Figure S3 in Supporting Information S1). The observed changes in stable isotope composition (up to 0.28‰ in δ^{18}O and 1‰ in δ^2H) were acceptable for most isotope hydrology research (Michelsen et al., 2018). The possible discrepancy with respect to rain event timing and amounts in our study was assessed using statistical methods (details in the Text S3 in Supporting Information S1), and the quality of the samples was evaluated by assigning four quality classes (QC1 to QC4):QC1 (n = 155): No or low maximum isotopic shifts ($\delta^{18}O < 0.28‰$ $\delta^2H < 1‰$) for high monthly precipitation volume (>6.3 mm);

QC2 (n = 20): Low estimated maximum isotopic shifts ($\delta^{18}O < 0.28‰$ $\delta^2H < 1‰$) but low monthly precipitation volume (<6.3 mm);

QC3 (n = 23): High estimated maximum isotopic shifts ($\delta^{18}O > 0.28‰$ $\delta^2H > 1‰$), but measured sample volumes (>6.3 mm) were higher than the monthly precipitation record, also with significantly depleted isotopic compositions and high d-excess.

QC4 (n = 16): High estimated maximum isotopic shifts ($\delta^{18}O > 0.28‰$ $\delta^2H > 1‰$) and low monthly precipitation volume (<6.3 mm) with extreme isotopic values and low d-excess.

The QC4 category samples were excluded from this study.

2.3. On-Site Measurements of Climatic Variables and Cyclone Records

Climatic variables, such as air temperature (T, °C), relative humidity (RH, %) and precipitation volume (mm), were continuously recorded at 10-min intervals by automatic weather stations situated near all rainfall collectors throughout the entire study period. The exception was PARA. For the PARA site, the weather data set at daily resolution was sourced from the Bureau of Meteorology (BOM, Paraburdoo Aero, no. 007185), which was 13.3 km from the rainwater collector. Historic cyclone pathways were extracted from the BOM Tropical Cyclone Database (Bureau of Meteorology, 2025), and cyclone months/seasons were defined as the month containing at least one cyclone, and these cyclone events accounted for >75% of rainfall in the month. The stratiform fraction was estimated using convective and total precipitation amounts derived from the ERA-Interim global atmospheric reanalysis (Copernicus Climate Change Service. 2023) with a temporal resolution of 3 hr and a spatial resolution of 0.25° by 0.25° (Figure 1 and Figure S2 in Supporting Information S1).

2.4. Determination of Local Meteoric Water Line

The monthly δ^2H and $\delta^{18}O$ values of rainwater were used to determine the Local Meteoric Water Lines (LMWL) for each site. Three regression methods, as recommended by Global Network Isotopes in Precipitation of the International Atomic Energy Agency, were used to calculate LMWL: the ordinary least squares regression (OLS), the reduced major axis regression (RMA), and the precipitation volume weighted least squares regression (PWLSR) as in Hughes and Crawford (2012).

Standard OLS regression model assumes zero error in the independent variable, which can be theoretically inconsistent given inherent analytical uncertainties. In contrast, RMA accounts for errors in both axes, offering a more geometric fit for bivariate data. Furthermore, PWLSR incorporates precipitation volume as a weighting factor, reducing the bias introduced by small, evaporatively enriched heavy isotope rainfall events that are less significant for groundwater recharge.

2.5. Modeling of the Stable Isotope Composition of Cloud-Base Vapor and Precipitation

The Rayleigh condensation formula is commonly used to infer the stable isotope composition of water vapor at a given height based on near-surface isotope data, assuming a purely moist adiabatic ascent leading to rainout (Deshpande et al., 2010; Wang et al., 2024):

$$\delta_{V\_C} = \left\{\left[\left(1 + 10^{-3}\delta_{V_G}\right) e^{-(\alpha-1)\left(\frac{z}{z_0}\right)}\right] - 1\right\} \times 10^3 \tag{1}$$

where δ_{V_C} is water vapor isotope compositions at the cloud base height and δ_{V_G} at the ground level, α is the equilibrium fractionation factor at the cloud base determined by temperature (Horita & Wesolowski, 1994), z is the cloud base height, which could be calculated by the Laplace pressure formula (Berberan-Santos et al., 1997, details in Supporting Information S1), and z_0 denotes the scale height of the atmospheric water vapor distribution (Parameswaran & Murthy, 1990).

Daily surface pressure data used to estimate cloud base height were extracted from the SILO repository (Jeffrey et al., 2001) (https://www.longpaddock.qld.gov.au/silo/). However, we did not measure the isotopic composition of ground-level vapor directly because of the remoteness of our locations. This could constitute a potential limitation for the estimation of sub-cloud evaporation. Nevertheless, to obtain a representative isotopic composition of vapor at ground level, the nudged Isotope-enabled model built from the Global Spectral Model (Iso-GSM) was run to extract monthly averages of δ_{V_C} for each site during the sampling period (2015–2024) (Yoshimura et al., 2008). For comparison, we also modeled the isotopic composition of vapor at ground level under the assumption that vapor was in isotopic equilibrium with local precipitation (δ_{P_G}) during rain events. This approach has been applied successfully in other subtropical regions characterized by atmospheric conditions close to saturation and with high air temperatures (>20°C) (Sinha & Chakraborty, 2020; Yao et al., 2018) (Figure S6 in Supporting Information S1). Estimation of rainfall evaporation by Stewart's model (1975) was improved to quantify the influence of sub-cloud evaporation on the stable isotope enrichment of falling raindrops compared with the isotope composition of precipitation at the cloud base (Froehlich et al., 2008; Salamalikis et al., 2016) (Equation 2):

$$\Delta_P = \delta_{P\_G} - \delta_{P\_C} = 10^3\left(1 - \frac{\gamma}{\alpha}\right)\left(f^{\beta} - 1\right) \tag{2}$$

where δ_{P_C} is the isotope composition of precipitation at the cloud base, γ and β are parameters depending on temperature and relative humidity at ground level (details can be found in Text S1 Equations S5–S8 in Supporting Information S1), and f is the remaining fraction of raindrops finally arriving on the ground. If the sub-cloud evaporation exists, Δ_P should be a positive value indicating the isotope enrichment.

In the isotope inversion model, δ_{P_C} is derived assuming isotopic equilibrium between δ_{P_C} and δ_{V_C} at the cloud base under thermodynamic conditions. Salamalikis et al. (2016) thoroughly discussed this basic assumption and its limitations. They are particularly useful for the preliminary evaluation of rainfall evaporation rates in regions with limited observation data, such as the Pilbara. However, we note that the remaining fraction of rainfall may be overestimated due to the equilibrium exchange process, which also enriches the rainfall isotope composition in heavy isotopes. This, in turn, could lead to underestimating the evaporative losses. Since the model represents a mixing process between the initial and final isotope compositions, it is still reasonable to compare isotope data across different seasons or sites. These comparisons offer a qualitative approach for evaluating local sub-cloud physical processes that influence the isotopic composition of raindrops (Wang et al., 2024; Zhu et al., 2021).

Additionally, a microphysical model, based on Wang et al. (2024), was implemented to provide a baseline for the outputs of the isotope inversion model. This model used meteorological variables, including temperature, relative humidity, rainfall amounts, rainfall intensity and surface pressure, to estimate the evaporative loss of raindrops (Text S1 Equations S9–S18 in Supporting Information S1).

Stewart's inversion model (1975) was used for monthly scale calculations based on δ^{18}O. Input parameters (air temperature, relative humidity, pressure) were extracted for each of 1,101 rainfall events during the observation 10-year period and weighted by rainfall volume to obtain monthly averages. The microphysical model was run separately to compute the event-based evaporative fraction, which was also weighted by rainfall amount to derive the monthly average.

2.6. Back Trajectory Analysis and Air Parcel Meteorological Data

Hybrid Single-Particle Lagrangian Integrated Trajectory (HYSPLIT) analysis was used to identify the precipitation history and moisture source for each rainfall event at the five sites during the sampling period. Codes in R studio were developed to run the HYSPLIT model by the NOAA Air Resources Laboratory (Stein et al., 2015). The input source area corresponded to the 1° × 1° area in the meteorological data set from the global data assimilation system (GDAS-1) (ftp://arlftp.arlhq.noaa.gov/archives/gdas1). Runtimes were set to be 120 hr backwards, and the arrival height was fixed to 1,500 m above ground level. These settings are based on previous studies conducted in similar geographic and climatic regions (Munksgaard et al., 2020; Zwart et al., 2018). For each rainfall event, a back trajectory was generated for each hour during the rainfall period and then processed to compute the average values. Before reaching the site, the cumulative precipitation along each trajectory was

10.1029/2025JD044431

calculated following Crawford et al. (2017) and reported as a monthly average to be paired with the monthly isotopic composition of rainfall.

A method based on Sodemann et al. (2008) was applied to identify and locate the potential moisture sources for each gridded point along the back trajectory. If the corresponding absolute humidity increased by more than 0.05 g/kg/h during the past 6 hr and the air mass was within the planetary boundary layer, the point was considered a source of moisture. The contribution of moisture from land and ocean sources along each trajectory was flux-weighted based on the net increase in absolute humidity at each point. Then, a $0.25° \times 0.25°$ hourly reanalysis data set (ERA5) from the European Center for Medium-Range Weather Forecasts (ECMWF) was interpolated for air temperature, relative humidity and evaporation rate from the selected source points (Hersbach et al., 2023). The retrieved variables were weighted in two steps. First, their mean values at land and ocean sources were estimated per trajectory, with values extracted from each gridded and weighted by their relative moisture contribution (net increase in absolute humidity over the past 6 hr). The second step involved converting the mean of variables per trajectory into a monthly average, weighted by event-based rainfall amount. Additionally, the isotopic composition of water vapor at source points was extracted from Iso-GSM and processed using the same weighted method.

3. Results

3.1. Characteristics of Rainfall Stable Hydrogen and Oxygen Isotope Compositions

The time series of monthly δ^{18}O and d-excess exhibited consistent intra-annual variability across the study period (Figure 2). The δ^{18}O values varied from −14.8 to 10.8‰, while the d-excess ranged from −39.4 to 18.2‰. Notably, the most positive (December 2022) and negative (January 2021) δ^{18}O and δ^{2}H, along with the lowest d-excess, were observed during cyclone months occurring in a negative IOD phase. Overall, the δ^{18}O and δ^{2}H values of rainfall during months influenced by positive IOD (the driest year of 2019) were higher than in the other periods (ANOVA, $P < 0.01$) except for ENSO affected months. In contrast, the d-excess values during positive IOD conditions were lower than those observed during negative IOD, ENSO and other periods ($P < 0.01$). Typically, the lowest isotope delta values were recorded for January, coinciding with the highest monthly totals, and showed an increasing trend toward maximum values in the driest months, consistent with the "amount effect." However, anomalies persisted, with high δ-values observed even during specific cyclone-affected months (e.g., December 2016, January and March 2019, December 2022, and April 2023) (Table S1 in Supporting Information S1).

The lowest arithmetic mean values (AM) and precipitation volume-weighted means (PWM) of δ^{18}O and δ^{2}H were observed at MARIL, and the highest AM and PWM of δ^{18}O and δ^{2}H were at KADA and ROBE, respectively (Figure 3, Table S2 in Supporting Information S1). Across all sites, AM were significantly higher than the PWM for δ^{18}O and δ^{2}H, confirming that low-volume events usually had higher δ-values than high-volume events. Moreover, among 39 samples with low d-excess values ranging between −10 and 0‰ in the entire data set, nine samples corresponded to large monthly rainfall volumes (>30 mm), 5 from KADA, 2 from ROBE and the other two from HD4 and MARIL. One cyclone rainfall sample (KADA: 122.4 mm) had an extremely low d-excess value of −24.67‰. Consequently, KADA had the lowest AM and PWM of d-excess (Table S2 in Supporting Information S1). However, a sensitivity analysis excluding this anomalous event aligned the site more closely with neighboring locations (e.g., PWM d-excess increased to 7.14‰; Table S3 in Supporting Information S1).

The highest difference between AM and PWM was observed during the cyclone season (difference of δ^{18}O between AM and PWM: −6.67‰), followed by the dry (−4.44‰) and wet (−3.88‰) seasons. For d-excess, AM values were significantly lower than PWM across all seasons (e.g., dry season: 7.83 vs. 11.10‰; wet season: 0.98 vs. 5.64‰; cyclone season: 7.59 vs. 8.81‰). The substantial AM-PWM discrepancy indicated significant seasonality in both rainfall volumes and isotope values, and considerable variation in sub-cloud evaporation processes across different rainfall events (Figure 3; Guan et al., 2013; Hollins et al., 2018).

Statistical analysis confirmed that while spatial differences between sites were insignificant ($p > 0.1$), temporal seasonal variations were significant (Figure 4). Specifically, the seasonal differences were more pronounced in δ^{18}O, with higher δ^{18}O and δ^{2}H in wet seasons than in dry and cyclone seasons at ROBE and HD4 ($p < 0.05$) (Figure 4a). Rainfall d-excess at PARA was significantly higher in the dry season than in the wet season (Figure 4b).

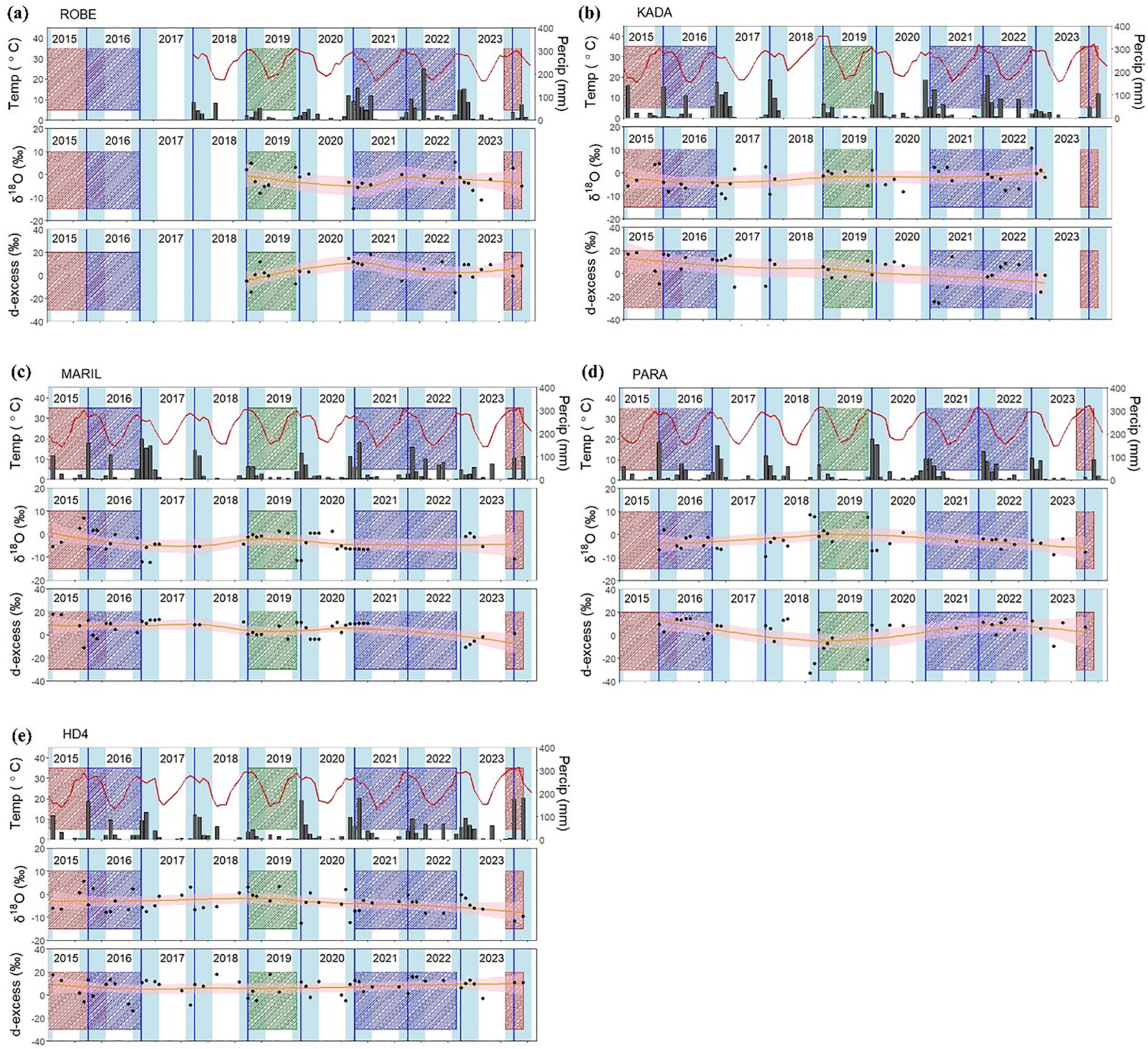

Figure 2. Time series of δ^{18}O and d-excess, temperature and precipitation at ROBE (a), KADA (b), MARIL (c), PARA (d) and HD4 (e). The orange lines and shades for δ^{18}O and d-excess represent the smoothed values and confidence intervals derived using the loess function implemented in R (R Core Team, 2021). Blue lines separate calendar years, and light blue shades represent the wet season. Red shading denotes periods of El Niño, green shading indicates phases of a positive Indian Ocean Dipole (IOD), and blue shading corresponds to negative IOD phases.

3.2. Local Meteoric Water Lines (LMWL)

To ensure statistical robustness, we compared LMWLs calculated using OLS, RMA, and PWLSR methods (Figure 5). For most sites (excluding KADA), OLS and RMA yielded slopes between 6.37 and 6.82, whereas PWLSR increased these slopes to >7.0. This shift confirms that unweighted regressions are significantly impacted by low-volume events evaporatively enriched in heavy isotopes. However, KADA presented a distinct pattern where all three methods yielded abnormally low slopes and intercepts. Excluding the anomalous February 2021 event increases the KADA PWLSR slope to 6.19 and intercept to −0.76 (Table S3 in Supporting Information S1), still remaining much lower than regional expectations. This deviated from earlier regional studies (Dogramaci et al., 2012; Skrzypek et al., 2019), which reported slopes closer to 7.0 for events >20 mm. Results for low-volume precipitation months (<20 mm) deviated from LMWLs and were usually characterized by more positive delta values, usually with lower d-excess (~50% of samples were below 0‰), suggesting that the kinetic fractionation caused by below cloud-base evaporation decreased PWLSR-LMWL slopes below the GMWL slope (Figure 5).

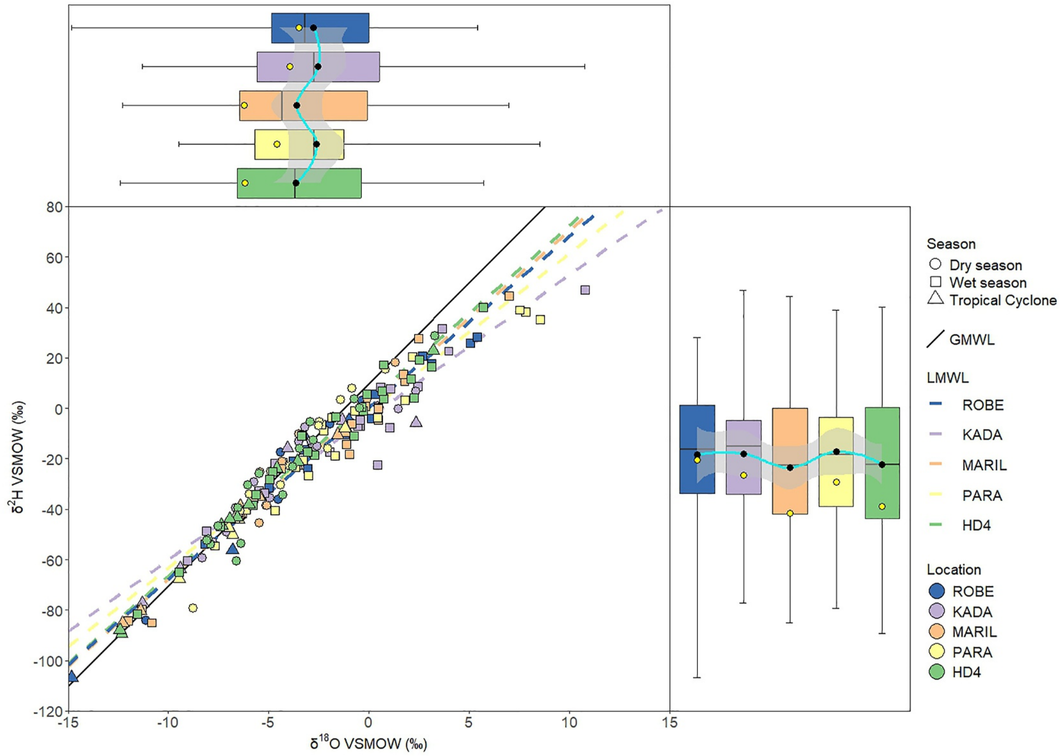

Figure 3. The Global Meteoric Water Line (GMWL) and the Local Meteoric Water Lines (OLS LMWLs) for each site. The box and whisker plots for $\delta^{18}O$ and $\delta^{2}H$ characterize the range of monthly values in the rain at each location. The box is drawn from Q1 (lower edge) to Q3 (upper edge) with a horizontal line (inside) denoting the median value. The boundaries of the lower and upper whiskers were the minimum and maximum values, respectively. Black points represent the average values, while yellow points represent the averages weighted by rainfall amount. The cyan line represents the smoothed values derived using the loess function implemented in the R package (R Core Team, 2021), showing the general variation of sites from coast to inland.

Cyclone precipitation yielded PWLSR slopes >7.0 at most sites (except KADA) and were consistently higher than those observed during dry and wet seasons (Figure S5 in Supporting Information S1). In ROBE, PARA and HD4, the LMWLs for both dry and cyclone seasons are closely aligned with the GMWL, indicating equilibrium fractionation during in-cloud condensation of vapor originating from seawater. Similar conditions were observed in high-volume rainfall samples at inland sites. In contrast, at KADA and near-coastal sites (ROBE), extreme rainfall events (>100 mm) exhibited unexpectedly lower slopes compared with moderate events (20–100 mm).

3.3. Sub-Cloud Evaporation Across Landscape Gradients

3.3.1. Stable Isotope Composition of Atmospheric Vapor

Atmospheric water vapor isotope compositions derived from Iso-GSM exhibited narrow ranges from −19.36 to −12.26‰ for $\delta^{18}O$ and −139.99 to −86.76‰ for $\delta^{2}H$ (Figure 6). While the model demonstrated qualitative consistency with the overall observed isotopic trends, its performance varied notably across different meteorological conditions. Specifically, Iso-GSM effectively captured the broad isotopic depletion in heavy isotope trends during high-volume, synoptic-scale events (such as cyclones). However, it tended to under-represent the localized, intense kinetic fractionation caused by sub-cloud evaporation during low-volume precipitation events in the dry season.

In contrast, the precipitation-equilibrium estimates of atmospheric vapor $\delta^{2}H$ displayed a much broader range of values, indicating a stronger influence of heavy isotope-enriched sources on local vapor. This pattern is consistent with contributions from the evaporation of persistent open water bodies on the ground surface (Figure S6 in Supporting Information S1). Under the driest initial conditions (RH < 40%), low-volume rainfall events (<30 mm) occurred over insufficient duration to support rain equilibration with the atmosphere, resulting in high

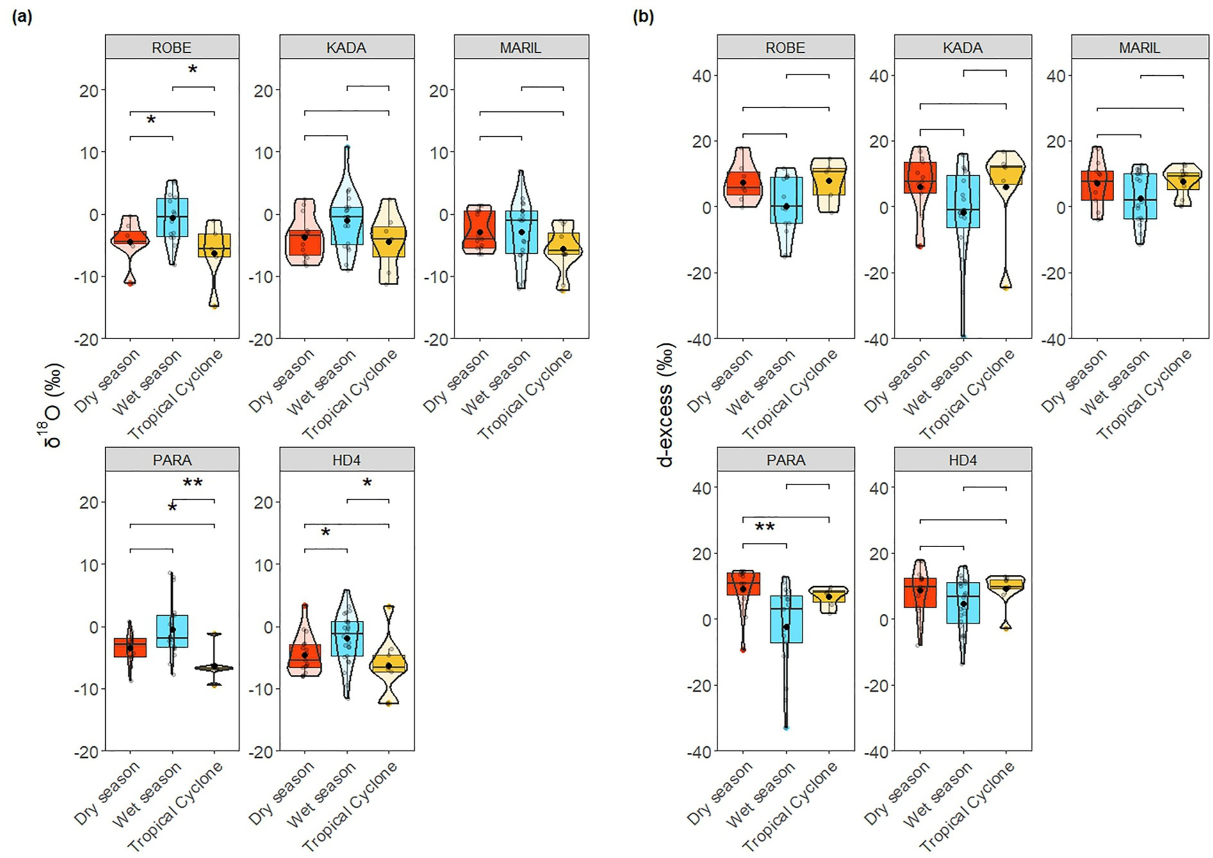

Figure 4. The box and violin plots show $\delta^{18}O$ (a) and d-excess (b) for the five sites grouped by wet, dry, or cyclone season. Black points in the boxplot denote the average values. A statistically significant difference was estimated using the Kruskal–Wallis post hoc Dunn test with Bonferroni adjustment comparing different seasons; star markers indicate $*p < 0.05$; $**p < 0.01$.

δ^2H signatures of vapor (suggested by Crawford et al., 2019). Consequently, precipitation-equilibrium methods were deemed unsuitable for calculating sub-cloud evaporation in this study. Most of the simulated Iso-GSM isotope delta values were plotted below the evaporation line, confirming that condensation and evaporation of raindrops significantly influenced δ^2H of subsequent precipitation. The distribution of monthly delta values for rainfall <50 mm was within the evaporation and Rayleigh distillation lines (nearly 95%). In contrast, >70% of heavy rainfall events (>50 mm) plotted below the Rayleigh line, attributing to the evaporation of falling rain near active convection instead of sub-cloud evaporation (Munksgaard et al., 2020). Two distinct clusters with exceptionally low δ^2H fell below the Rayleigh line: one associated with dry-season sub-cloud evaporation, and another with heavy wet/cyclone season rain, likely derived from evapotranspiration or soil moisture sources characterized by low δ^2H.

3.3.2. Sub-Cloud Evaporative Losses

The evaporated fractions of raindrops (F_E) were calculated using the Stewart model discussed in Section 2.4, based on vapor isotope composition from Iso-GSM (Figure 7). Generally, F_E had a large range of variation from 0.2% to 76% with a mean value of 30.6 ± 2.2% (95% CI). KADA had the highest mean value of F_E (32.4 ± 2.3%), while the lowest was at ROBE (28.4 ± 2.9%). However, no significant differences in F_E between sites were found due to high variance, suggesting similar but variable evaporative conditions at all five sites. However, seasonal differences were pronounced: inland sites showed significantly higher evaporative losses in the wet season compared with the dry season (Figure 7). The significant seasonal differences in the evaporative fraction were consistent with the seasonal variations in d-excess (Figure 4b) and the stratiform fraction of rainfall. At inland sites, the stratiform precipitation accounted for ~70% of rain events, on average, in the wet season, while convective precipitation dominated mostly in the dry season (Figure S2 in Supporting Information S1). Higher air

10.1029/2025JD044431

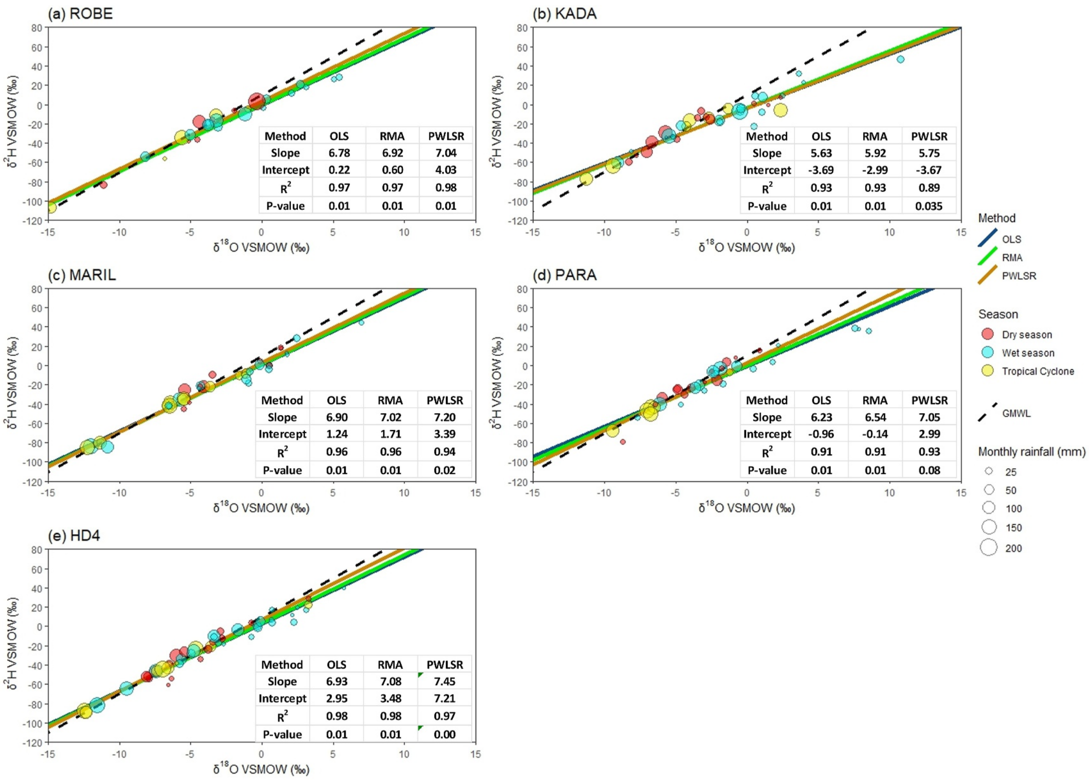

Figure 5. Regression models for the δ^{18}O-δ^2H relationship using ordinary least squares regression (OLS), reduced major axis least squares regression (RMA), and precipitation weighted least squares regression (PWLSR) at ROBE (a), KADA (b), MARIL (c), PARA (d) and HD4 (e) sites. The slope, intercept, R^2 and P-values were shown in tables. Monthly rain points were colored by season and point size indicated the monthly rainfall volume. The Global Meteoric Water Line (GMWL) was plotted as a dashed line.

temperatures and lower relative humidity during rainfall led to more intense evaporation, resulting in kinetic fractionation that decreased the d-excess in the remaining liquid.

A sensitivity analysis was performed to assess seasonal changes in variables influencing evaporation using long-term average climate and stable isotope data during the rain periods (shown in Table S4 in Supporting Information S1). The $\pm 10°$C changes in the mean air temperature (18.5 and 26.8°C for dry and wet seasons) and $\pm 10\%$ changes in relative humidity (69% and 63% for dry and wet seasons) resulted in only a small difference (<5%) in the estimated evaporative fraction. Additionally, the potential discrimination of 0.3‰ variation in rainfall δ^{18}O also had minimal impact on the calculated evaporative losses (<5%). This finding suggests that potential isotope changes in water samples due to secondary evaporation in the rain collector before sample extraction were unlikely to result in a substantial overestimation of sub-cloud evaporation. In contrast, uncertainty in the input values of the stable isotope composition of estimated water vapor had a more significant impact on the F_E calculations. A ± 2.5‰ uncertainty in the estimated water vapor δ^{18}O could cause up to -12% to 15% variations in F_E values (up to ~79% difference from the original value). Therefore, accurately estimating F_E or quantifying evaporative losses from raindrops becomes challenging because of the uncertainty of the estimation of the vapor stable isotope composition. However, continuous vapor measurement at the ground level at remote locations over an extended period is impossible either at the ground or at the cloud base. Regardless of this limitation, the independent microphysical model showed significant consistency ($r = 0.41$, $p < 0.001$) with our Iso-GSM-based estimates, supporting the validity of the calculated evaporative losses (Figure S7 in Supporting Information S1).

3.4. Back Trajectory of Air Parcels Prior to Rainfall

The HYSPLIT model was employed to trace air parcel movements over 120 hr spatial trajectory, track precipitation accumulation before reaching each study site, and identify the moisture sources associated with each rainfall event. A total of 1,101 air parcel trajectories corresponding to 1,101 rain events at five sites over the study

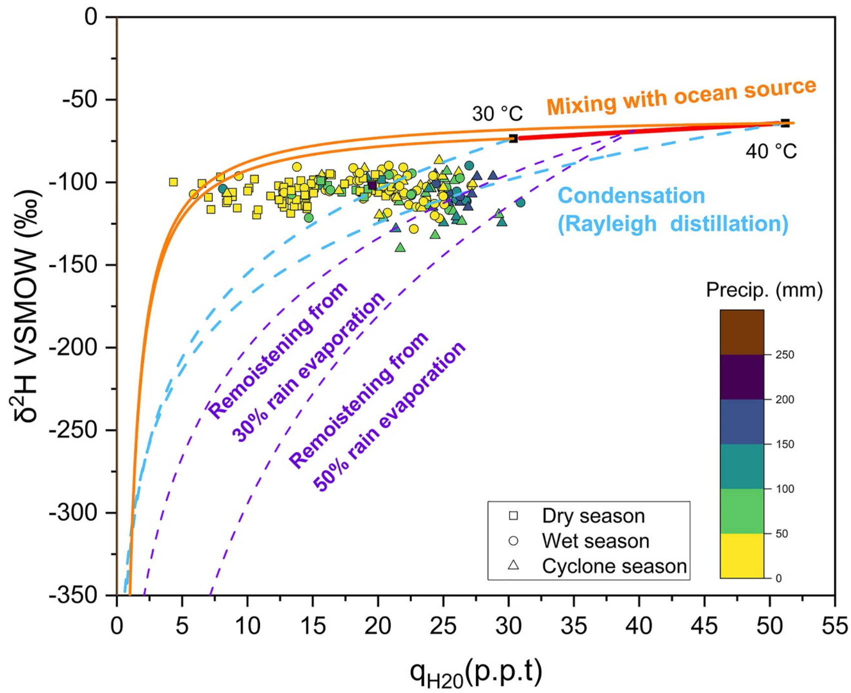

Figure 6. Scatter plots of monthly δ^2H values of water vapor (from the Iso-GSM scheme) versus water volume mixing ratio (qH_2O) were calculated based on local meteorological observations. The shapes of the scatter points reflect the seasons, and the colors reflect rainfall volume. Theoretical predictions, where δ^2H values are a function of qH_2O, are adapted from Noone (2012). The dashed orange curve represents evaporation and mixing with vapor depleted in heavy isotopes; these vapors equilibrate with tropical ocean water at temperatures ranging from 30°C to 40°C. The cyan curves represent the Rayleigh distillation model (condensation) originating from saturated oceanic vapor (80% RH) at air temperatures between 30°C and 40°C. The purple lines represent the process of raindrop evaporation into the atmosphere, indicating stable isotope exchange. The analysis is based on mass and isotope balance models incorporating variable evaporation ratios ranging from 30% to 50%.

period were backtracked (Figure S8 in Supporting Information S1). Notably, air parcels originating from higher latitudes followed longer trajectories over 120 hr observation window, suggesting higher velocity. They were depleted in atmospheric moisture, a typical pattern observed during the dry season and in directions arriving from other directions. In contrast, most air parcels from the ocean's northern and northwestern tropical parts retained high moisture concentrations during the wet season. Air masses from eastern Australia and the Southern Ocean were associated with lower moisture content, especially during cyclone months (Table S5 in Supporting Information S1). Overall, the precipitation history of air trajectories varied across sites, with more moisture originating from the Australian continent being supplied to air masses during the wet season compared to the dry season. The frequency of potential moisture source locations indicated that moisture uptake overland along air parcel tracks was more significant during the wet and cyclone seasons than during the dry seasons, likely due to higher moisture availability and higher evaporation over land during the summer season (Figure S9 in Supporting Information S1). The enhanced feedback of terrestrial evapotranspiration to rainfall, driven by strong winds, likely contributed to δ^{18}O decrease in water vapor and further increased the d-excess downwind, which has been observed in some other sub-tropic regions (Xia et al., 2021; S. Xu et al., 2023). This process, particularly, could occur after a rainstorm or cyclone event, delivering low delta precipitation values anyway and creating a significantly depleted source of heavy isotopes evaporating from the ground-level water (Figure 6).

3.5. Relationship Between Rainfall Stable Isotope Compositions and Weather Parameters

3.5.1. Local Variables

Rainfall δ^{18}O correlated significantly with relative humidity, vapor pressure deficit (VPD), rainfall amount, the proportion of small rain volume in monthly total, and the fraction of sub-cloud evaporative losses (Table S11 in Supporting Information S1). Correlations between δ^{18}O and air temperature were only found to be significant but

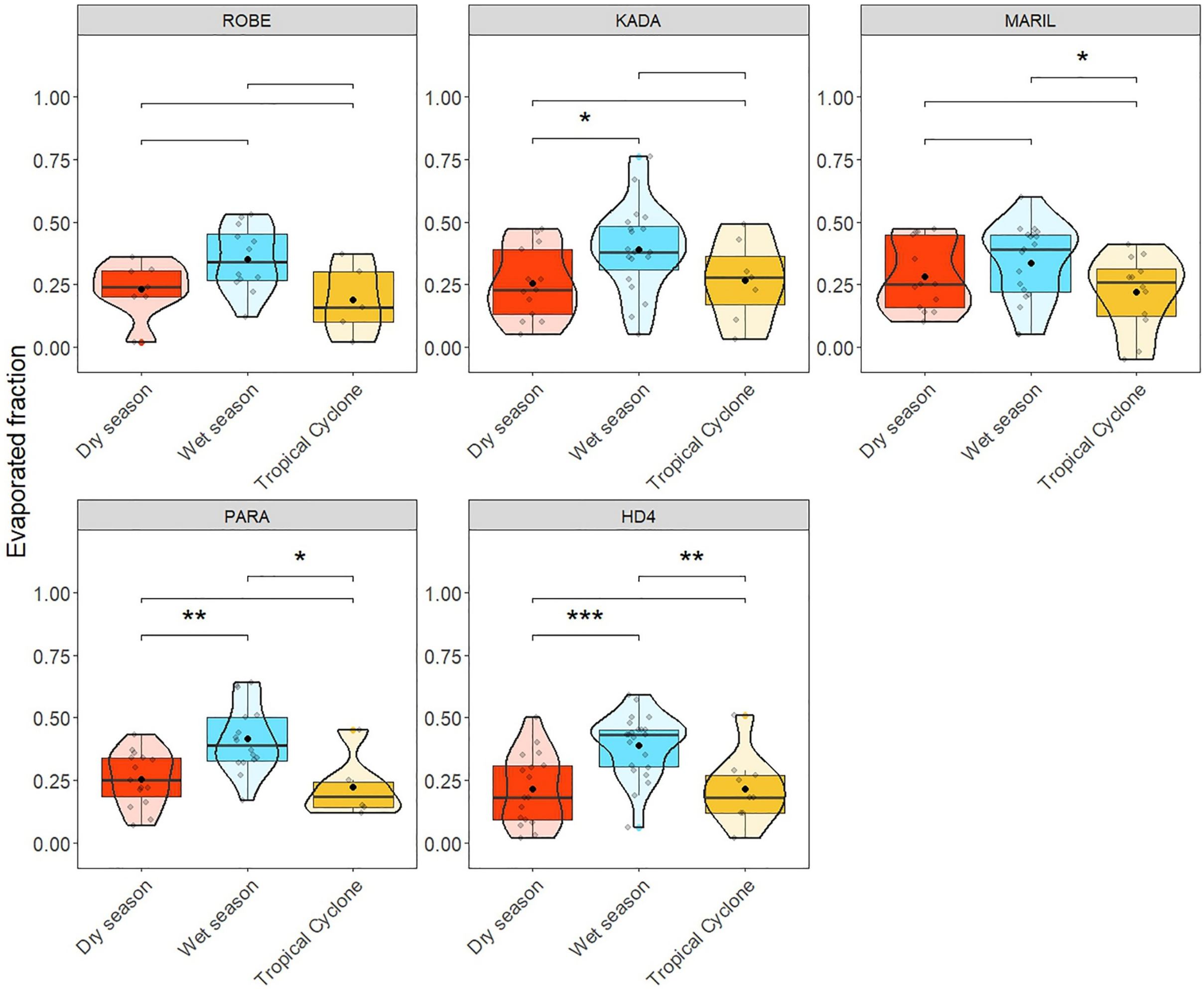

Figure 7. The box and violin plots describe the distribution of evaporated fractions of raindrops (F_E) across seasons, as estimated using the Stewart model and water vapor isotope delta values (data from Iso-GSM). Black points in the boxplot denote the average values. Significant differences, confirmed by the Kruskal–Wallis post hoc Dunn test with Bonferroni adjustment, between different seasons are marked with stars as follows: *$p < 0.05$; **$p < 0.01$; and ***$p < 0.001$.

weak at ROBE ($r = 0.44$). This lack of correlation agreed with Landshuter et al. (2024), who attributed low inter-seasonal variability to the minor role of surface temperature influence on stable isotope signals.

While precipitation type often governs isotopic variability in the tropics, we found no significant correlation between stratiform fraction and rainfall δ^{18}O at most sites. δ^{18}O variability was more positively correlated with the stratiform fraction in ROBE and KADA ($P < 0.05$), coinciding with a weaker "amount effect." At the other four sites, the "amount effect" dominated, showing stronger correlations with rainfall amount than with stratiform fraction. MARIL and HD4 displayed the strongest "amount effect," whereas rainfall intensity showed no significant relationship with isotopic composition.

Longer rainfall durations were associated with lower δ^{18}O (KADA, PARA and HD4) values and higher d-excess (all sites except ROBE) in the rain, suggesting overall lower under-cloud-base evaporation (Tables S11 and S12 in Supporting Information S1). Additionally, the duration of rainfall events showed a stronger positive correlation with d-excess than with δ^{18}O (higher $|r|$ values), while the stratiform fraction of precipitation was not positively related to rainfall duration ($p > 0.1$). The proportion of rainfall volume from events <5 mm also had a notable impact on δ^{18}O and d-excess in most sites. These findings also highlighted the importance of sub-cloud evaporation, which showed the highest correlation with δ^{18}O and d-excess values (Tables S11 and S12 in Supporting Information S1). This was also supported by the significant correlation between d-excess and relative humidity (as well as VPD).

Seasonally, sub-cloud evaporation was the primary driver of dry season δ^{18}O at all sites except KADA. Correlations between δ^{18}O and multiple local variables strengthened in the wet seasons. The KADA site remained distinct, with δ^{18}O consistently sensitive to RH, VPD, and the proportion of small-volume events (<5 mm).

3.5.2. Regional Variables

Back-trajectory analysis (Tables S5 and S6 in Supporting Information S1) confirmed a strong "rainout effect" for δ^{18}O at all sites except ROBE and KADA, with δ-values correlating with cumulative upstream rainfall (Tables S12 and S13 in Supporting Information S1). In contrast, d-excess showed a markedly stronger correlation with the proportion of moisture originating from terrestrial sources than with rainfall δ^{18}O. At PARA and HD4, both located more than 270 km inland, the d-excess of monthly rainfall was significantly correlated ($p < 0.01$) with both the d-excess of atmospheric vapor and evaporation rates at terrestrial moisture source regions. This finding highlights the role of continental recycling and re-evaporation in shaping inland isotopic signatures (Crawford et al., 2023).

4. Discussion

4.1. Main Drivers of Stable Isotope Composition Variability in Precipitation

4.1.1. Principal Component Analysis

PCA (Figure 8) reveals that stable isotope variability in the Pilbara is not driven by a single overarching linear factor. The first two principal components (Dim1 and Dim2) explain 45.7% of the total variance. Dim1 (31%) is primarily associated with local humidity, vapor pressure deficit (VPD), sub-cloud evaporative fraction, and the stratiform fraction of rainfall. In contrast, Dim2 links to air temperature, precipitation intensity, and meteorological conditions at the moisture source. Parameters such as local precipitation, cumulative precipitation before the cloud arrived at the study site, and relative humidity in the continental moisture source area contributed to both Dim1 and Dim2.

Critically, the temperature vector is orthogonal to the isotopic vectors, indicating a decoupling of temperature from isotope composition. This is in contrast to temperate climates, where temperature dominates seasonal variability in stable isotope composition (Rozanski et al., 1992). There were a number of high-volume precipitations close to the temperature vector, indicating that temperature-dependent controls on rainfall isotopic composition only occurred during intense convective events, related to the cloud microphysical process, for instance, equilibrium fractionation of in-cloud condensation with strong updrafts (Crawford et al., 2023; Hu et al., 2018). This analysis highlighted that high rainfall δ^{18}O and δ^{2}H values were positively related to sub-cloud evaporation, the proportion of small rain volumes, and moisture contribution originating from land sources. Furthermore, sub-cloud evaporation strongly correlated with the stratiform fraction as well as the proportion of small rainfall volumes (Table S14 in Supporting Information S1). The stratiform fraction possessed a positive function for sub-cloud evaporation, which tended to increase rainfall δ^{18}O and δ^{2}H and weaken the "amount effect" as found in ROBE and KADA.

4.1.2. Precipitation Activity Type Controls Sub-Cloud Evaporation

Stratiform precipitation frequently occurs in near-coastal areas following cyclones or mesoscale convective complexes (Schumacher & Houze, 2003). Stratiform rainfall also predominantly characterizes wet seasons in inland regions, while it is uncommon during dry seasons (Figure S2 in Supporting Information S1). The high spatial variability of precipitation patterns becomes especially important to recognize. To our knowledge, the underlying drivers of this variability have not been previously examined in subtropical regions with semi-arid climates.

Most stratiform precipitation, characterized by smaller rain volumes, was observed along the positive *x*-axis (Figure 8b), suggesting that it was more influenced by sub-cloud evaporation compared to convective precipitation when rain amounts were at the same level. Although a few convective precipitations were also evaporative dependent, situated in quadrants 1 and 4, which were likely related to higher proportions of small rainfalls.

Sub-cloud evaporative loss correlated significantly with stratiform fraction ($r = 0.38$, $p < 0.001$). Despite the increased stratiform rainfall proportions, they did not correspond to higher small rain proportions or longer rain

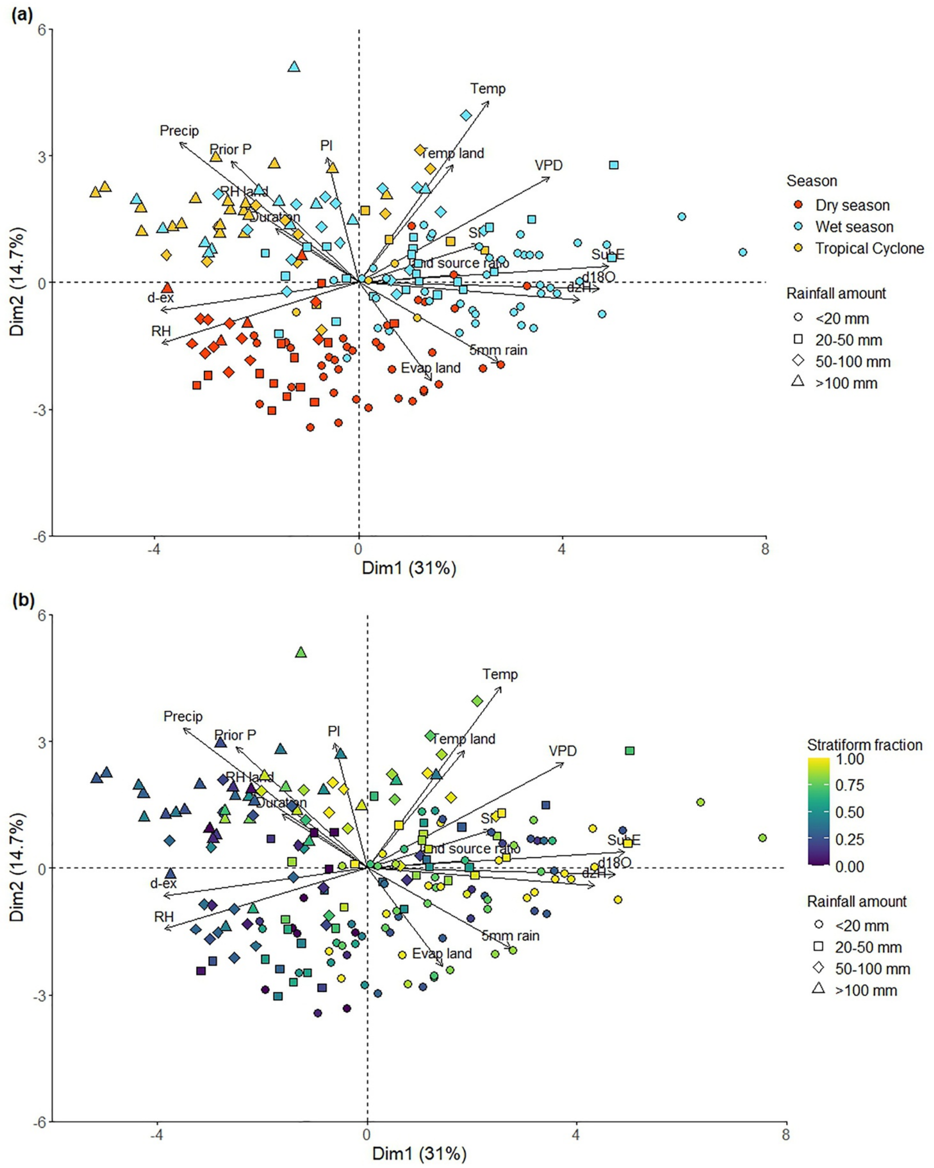

Figure 8. The PCA biplot shows monthly rainfall by season with the classification of rainfall amount and overlain by vector loadings from the score plot for major variables tested in the analysis, (a) color-coded by season; (b) color-coded by a monthly stratiform fraction. Variable abbreviations: d18O—δ^{18}O of rainfall (‰); d2H—δ^{2}H of rainfall (‰); d -ex—d -excess (‰); Temp—air temperature (°C); RH—relative humidity (%); Precip—rainfall amount (mm); VPD—vapor pressure deficit; PI—rainfall intensity (mm/h); duration—rain duration (h); 5 mm rain- Proportion of rain (<5 mm) contribution; SubE—sub -cloud evaporative fraction; Prior P—previous cumulative precipitation along the trajectory (mm); land source ratio- moisture source from land; Temp land- average temperature of moisture source from the land; RH land- average relative humidity of moisture source from land (%); Evap land- average evapotranspiration of moisture source from land (mm); SF—stratiform fraction.

durations (no significant correlations, $p > 0.1$). Stratiform rain was often characterized by small raindrops (∼1 mm diameter), leading to greater susceptibility to evaporation (Lekshmy et al., 2018). Besides, increased travel time from the cloud base to the ground surface in stratiform rain could intensify raindrop re-evaporation and isotopic exchange with below-cloud vapor even at low temperatures and in humid areas; therefore, the increased sub-cloud evaporation masked the "amount effect" and "rainout effect" (Prein, 2022).

Inland sites (KADA, PARA, HD4) exhibited distinct seasonality, where higher stratiform fractions in the wet season coincided with elevated sub-cloud evaporation (Figure 7). Uniquely at KADA, sub-cloud evaporation during the cyclone season remained high (mean 27%), significantly exceeding the average of other sites (mean 21%). Notably, higher δ^{18}O with extremely low d-excess values (<−16‰) were observed in four moderate rain months (17.8–122.4 mm) influenced by shallow convective systems (in/after cyclone season). These observations support recent findings that re-evaporation in shallow convection drives heavy isotope enrichment (Landshuter et al., 2024), challenging the traditional view that organized systems invariably yield low δ-values (Aggarwal et al., 2016). In contrast, the nearby MARIL site experienced colder conditions and shorter raindrop falling times (Table S7 in Supporting Information S1). This limited the isotopic exchange between raindrops and atmospheric vapor (Misumi et al., 2021). Therefore, the heavy isotope enrichment in rainfall at the ground level as well as the relationship between isotope variability and stratiform fraction would be reduced, eventually producing lower PWM values for δ^{18}O and δ^{2}H but a higher PWM value for d-excess in MARIL (Table S2 in Supporting Information S1).

Despite similar wet-season stratiform fractions at KADA, PARA, and HD4, the prevalence of low-volume rainfall at KADA amplified total droplet evaporation. Anomalously high δ^{18}O but lower d-excess in large-volume monthly composite rainfall led to a lower slope and intercept of the LMWL at KADA. This suggested that kinetic fractionation caused significant changes in δ^{18}O and δ^{2}H of the ground-level raindrops, which diminished the impact of precipitation amount.

Excluding KADA, the results reveal a clear regional trend: the "amount effect" and "rainout effect" strengthen with increasing annual precipitation across the remaining transect (ROBE-PARA-MARIL-HD4). Additionally, correlations between δ-values and rainfall-related variables strengthened as precipitation increased (Table S11 in Supporting Information S1). This can be attributed to the largest rainfall events, which are often linked to cyclones associated with negative isotope anomalies, consistent with studies from eastern coastal Australia (Crawford et al., 2023; Munksgaard et al., 2020).

4.1.3. Moisture Sources for Landfall Precipitation

Back-trajectory analysis reveals significant terrestrial moisture recycling, contributing 35% (dry season) to 47% (wet season) of total moisture. This aligns with eastern Australian estimates (~40%; Crawford et al., 2017) but exceeds previous findings for the northwest (23%; Holgate et al., 2020). Higher proportions of stratiform precipitation were more closely related to terrestrial moisture contributions at KADA ($r = 0.34$, $p < 0.05$), highlighting the role of regional evapotranspiration (Yang & Smith, 2008). Southern Indian Ocean surface waters had significantly more positive δ-values and had higher d-excess (average: δ^{18}O: 0.094‰, d-excess: −0.46‰; Reverdin et al., 2022) compared to terrestrial surface water (average δ^{18}O − 4.40‰, d-excess −2.00‰) and soil water (average: δ^{18}O < 0‰) (Dogramaci et al., 2012; Skrzypek et al., 2019). While groundwater is distinctively depleted in heavy isotopes (average: δ^{18}O − 8.02‰, d-excess 8.56‰), its contribution to atmospheric vapor is negligible due to usually thick unsaturated zone (Skrzypek et al., 2019). Moisture derived from land evapotranspiration was typically characterized by lower delta values and d-excess in water vapor compared with moisture originating primarily from seawater evaporation. This land-sourced moisture contributed to reduced d-excess signatures in rainfall when more than 70% of the moisture originated over land, particularly during the wet season (Table S6 in Supporting Information S1). This effect is amplified in the wet season, where higher temperatures and lower humidity intensify terrestrial evaporation, further depressing the d-excess of land-sourced vapor (Table S6 in Supporting Information S1).

4.1.4. Water Vapor Recycling

Moisture recycling likely played a key role in driving the high PWM d-excess in rainfall at the highlands (HD4) (Table S2 in Supporting Information S1), while the sub-cloud evaporation rate remained similar to other sites. Given that the contribution of ocean-sourced moisture with high d-excess to local rainfall was limited during the wet season, a significant portion of the convective precipitation was likely sourced from rainfall evaporating near convective clouds, estimated to account for 20%–50% of the initial rainfall volume (Worden et al., 2007). As a result, intense convection further fed isotopically depleted vapor into the cloud (updraft), amplifying the effect of moisture recycling and contributing to the observed effect in downwind precipitation.

Also, the average precipitation volume-weighted d-excess at HD4 (10.62‰) was similar to the mean vapor d-excess at the terrestrial moisture source (11.0‰), indicating a significant portion of precipitation derived from evapotranspiration (Froehlich et al., 2008). On the other hand, diffusive exchanges would combine the d-excess of rain droplets with local recycled ambient vapor, making d-excess more positive. d-excess in precipitation often displays an increasing trend with altitude associated with convective activities (Adhikari et al., 2024). Moisture recycling was not dominant at PARA, the inland site at a lower altitude (~424 m a.s.l.), in contrast to HD4 (717 m a.s.l.) despite similar precipitation conditions. Vertical moisture mixing during stratiform rain events was restricted compared with dominant convective precipitation (Lekshmy et al., 2018). The local moisture recycling would also lead to a higher slope intercept of LMWL at HD4 (Crawford et al., 2013).

4.2. Influence of the Monthly Rainfall Sampling Scheme on Characterizing Isotopic Signatures in Precipitation

Standard GNIP/IAEA protocols rely on monthly composite sampling to derive volume-weighted mean isotopic values. While efficient, this approach faces challenges in semi-arid regions where collected samples are subject to potential evaporation and fractionation during extended holding periods (Arellano et al., 2024; Natali et al., 2024). Our research highlights a critical nuance: the internal structure of a monthly sample, specifically the proportion of low-volume events, can yield distinct isotopic signatures even when total monthly rainfall appears identical (Table S8 in Supporting Information S1). For example, a single 100 mm rainfall event from a cyclone typically yields more negative δ-values, whereas the same total volume distributed across five or more smaller events (each <20 mm) tends to produce more positive δ-values.

Misinterpreting these high-volume months characterized by elevated δ-values can obscure the true "amount effect" and Local Meteoric Water Line (LMWL). This is evident at KADA, where we identified two distinct groups of monthly samples with totals >50 mm during the cyclone season.

The first group, with high $\delta^{18}O$ values (mean −4.43‰), received an average of 27% of its volume from >10 mm rainfall events. The second group, with significantly lower $\delta^{18}O$ (mean −11.68‰), was dominated by larger events (only 34% from small precipitation events with volume <20 mm). Despite statistically similar total volumes ($p > 0.2$), the first group had elevated δ-values. This confirmed that the contribution of sub-cloud evaporation from small events (see Section 4.1.2) can significantly increase the δ-value of the final composite sample, lowering the d-excess.

However, interpreting LMWLs in semi-arid environments remains challenging due to the nature of monthly composite sampling. These physical samples inherently aggregate extremely low-volume events that have undergone intense sub-cloud evaporation, and their disproportional contribution to mean stable isotope delta values can persist even when applying precipitation-weighted statistical methods such as PWLSR. Since these small events have minimal impact on dryland water budgets, they should ideally be excluded to avoid biasing long-term weighted means, as suggested by previous studies (Hollins et al., 2018; Hughes & Crawford, 2013). Previous research has also highlighted a small but statistically significant difference between the means of δ-values from weekly and daily rain sampling (Crawford et al., 2023). Using Monte Carlo simulations, we conceptually demonstrated how varying proportions of small rainfall events within high-volume monthly totals can influence the isotopic composition of composite rainfall samples (Figure S10 in Supporting Information S1). These variations can lead to distinct PWLSR-LMWLs. In arid and semi-arid conditions, precipitation events under 10 mm or even more were usually excluded to avoid hydrologically unrepresentativeness of an LMWL for local conditions (Wang et al., 2018) as removing small rain events (daily) would increase the slope. While removing monthly samples affected by small rain events would produce an LMWL slope comparable to event-based or daily LMWLs where low-volume precipitation is deliberately excluded, this would also lead to the exclusion of a substantial proportion of the monthly data set. To address this issue, we propose a new precipitation volume "cut-off" approach to identify the potential influence of small-volume rainfalls on LMWL and weighted mean values (Figure 9 and Figure S11 in Supporting Information S1). The volume threshold for small rainfalls was set between 1 and 30 mm, with increments of 1 mm. The LMWLs were calculated in steps, gradually excluding samples with a cumulative volume of small rainfall of more than 0%, 20%, 40%, 60%, or 80% of the total monthly rainfall. Small rain events significantly contributed to the monthly rainfall samples across the five sites. The exclusion of monthly samples with more than 40% of monthly rainfall from <5 mm events resulted in the removal of 40% of the total samples.

Unfiltered PWLSR calculations typically yield lower LMWL slopes and higher weighted mean δ-values due to the influence of enriched in heavy isotopes low-volume events. Excluding monthly samples where small rains (<5 mm) constituted >40% of the total volume significantly increased LMWL slopes (notably at HD4) and

10.1029/2025JD044431

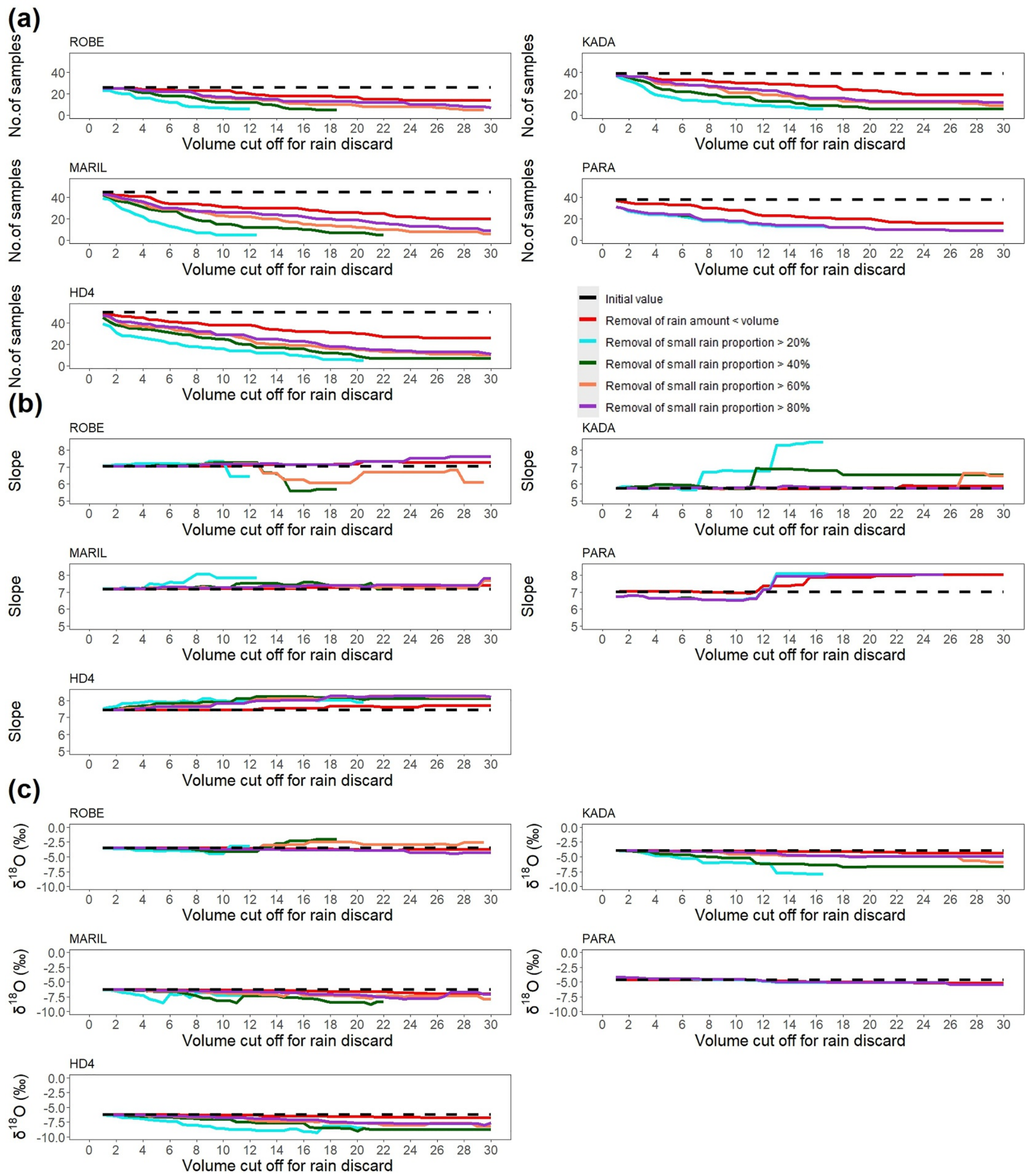

Figure 9. LMWL- PWLSR models were repeatedly calculated excluding small rains; only mean monthly samples above the selected minimum precipitation volume threshold were used for each calculation round to explore changes in slope and δ^{18}O: (a) the number of samples above the selected threshold; (b) the slopes of LMWL- PWLSR for samples above the threshold; (c) volume-weighted mean δ^{18}O for samples above the threshold. The slopes of LMWL and weighted means were calculated only when the number of remaining samples was more than five.

decreased weighted mean δ^{18}O across most sites, confirming the effective removal of evaporative signals. Additionally, increasing the criteria for small rain and lowering the threshold for the cumulative proportion of small rain in the filtering process both altered the weighted mean d-excess (Figure S11b in Supporting Information S1) across the five sites and decreased the weighted mean δ^{18}O (Figure 9c) with the exception of the near coast site ROBE, where δ^{18}O instead increased, likely because removing small rain events unmasked the dominance of enriched in heavy isotopes oceanic storms. The impact of this "cut-off" approach was most profound at KADA. Filtering months dominated by <5 mm rain shifted the PWLSR slope from 5.76 to 6.0, while increasing the mean d-excess by 1.71‰. Applying a stricter threshold (removing months dominated by

<11.5 mm rain) sharply raised the slope to 6.92, aligning it with event-based expectations, though this reduced the effective data set from 39 to 14 samples.

Small rainfall events <20 mm contributed negligibly to soil moisture storage or groundwater recharge (Dogramaci et al., 2012; Skrzypek et al., 2019). However, they disproportionately affected the isotopic record. In our study, 41.4% of all monthly samples were <20 mm. More critically, even among high-volume months (>50 mm), 61% contained a significant proportion (>40%) of small, evaporated rain events, which resulted in substantially varied isotopic signatures (Table S8 in Supporting Information S1). This introduces substantial uncertainty when using standard monthly composites to trace groundwater sources, as the isotopic signal of effective recharge is obscured by non-recharging, enriched rainfall. A review of reported monthly rain data used in previous hydrological tracing or modeling is recommended. We acknowledge that the specific "cut-off" threshold is site-specific and requires validation in diverse hydroclimatic settings using high-resolution event-scale observations.

5. Conclusions

The 10-year monthly rain sampling program in the Pilbara provides a comprehensive evaluation of the meteorological drivers controlling stable isotope variability. Low δ-values of rainfall were primarily driven by the "amount effect," with high δ-values and low d-excess characterizing positive IOD phases (e.g., 2019). However, at coastal sites where this effect was weak, isotopic enrichment correlated positively with the stratiform fraction, highlighting the role of cloud microphysics. Sub-cloud evaporated fraction of raindrops varied widely across sites and seasons, ranging from 0.2% to 76%, with a 10-year average of 30.6 ± 2.2%. High evaporative losses were intrinsically linked to stratiform precipitation and shallow convective systems during cyclone months. These processes enriched raindrops in heavy isotopes (lowering d-excess) and flattened the slope of the Local Meteoric Water Line (LMWL). Terrestrial moisture recycling was a critical driver, contributing 47% of moisture in the wet season compared with 37% in the dry season. This terrestrial input, dominated by evapotranspiration, typically lowered the $\delta^{18}O$ and d-excess of rainfall, though intense inland convection can locally amplify d-excess via recycling.

A critical methodological outcome of this study is the demonstration that standard monthly composite sampling in semi-arid environments was systematically biased by low-volume rainfall events, characterized by high delta values due to under-cloud evaporation preferentially removing light isotope from the remaining liquid phase. Because these minor events rarely overcome soil moisture deficits to contribute to groundwater recharge, their inclusion obscured the true isotopic baseline of the hydrological system. We proposed a volume-based "cut-off" approach to filter this bias, yielding more robust LMWLs and weighted means for semi-arid regions to reflect the water available for terrestrial recharge.

While this study identified the key drivers of isotopic variability, a fully quantitative link between microphysical processes and the rainfall isotope patterns requires further verification. Future work should focus on simultaneous measurements of precipitation and vapor isotopes coupled with cloud-based monitoring to empirically test the kinetic fractionation mechanisms proposed here. Future projections suggest an increasing frequency of the synoptic systems producing heavy rainfall in the Pilbara region (Clark et al., 2018). However, the seasonal distribution of this precipitation remains uncertain, making its impact on deep soil moisture retention difficult to predict (Skrzypek et al., 2019). In some parts of Australia, rain has become more frequent but shorter in duration, which increases susceptibility to higher under-cloud evaporation and may reduce overall moisture availability (Dey et al., 2020). Accurately quantifying the strength of soil moisture-vegetation-rainfall feedback mechanisms at large spatial scales and short temporal intervals is also recommended (Wierik et al., 2021).

Conflict of Interest

The authors declare no conflicts of interest relevant to this study.

Availability Statement

The original data set with monthly stable isotope composition was generated during this study and it is available as Supplemental Material from the publisher's website as an electronic attachment: Supplementary_pilbara_rainfall.xlsx (https://doi.org/10.6084/m9.figshare.31517590) (Wan et al., 2026). Historic cyclone pathways were extracted from the BOM Tropical Cyclone Database (Bureau of Meteorology, 2025). The stratiform fraction was estimated using convective and total precipitation amounts derived from the ERA-Interim global atmospheric reanalysis (Copernicus Climate Change Service, 2023). Daily surface pressure data used to estimate cloud base height were extracted from the SILO repository (Jeffrey et al., 2001) (https://www.longpaddock.qld.gov.au/silo/). The input source data for Hybrid Single-Particle Lagrangian Integrated Trajectory (HYSPLIT) analysis was from the global data assimilation system (GDAS-1) (ftp://arlftp.arlhq.noaa.gov/archives/gdas1).

Acknowledgments

This research was conducted in partnership with Rio Tinto (RTIO) and supported by the Australian Research Council (LP210300691). We are grateful to our RTIO and The University of Western Australia (UWA) teams, whose contributions made this study possible. We also thank Marillana Station operators, including Sue and Lee Bickell, and Jean Paplauskas, who volunteer to collect monthly samples. Open access publishing facilitated by The University of Western Australia, as part of the Wiley - The University of Western Australia agreement via the Council of Australasian University Librarians.

References

Adhikari, N., Gao, J., Yao, T., Puri, A., Chen, M., & Zhao, A. (2024). The influence of moisture transport processes on the stable isotopic compositions in precipitation on the South slope of the Himalayas. *Global and Planetary Change*, *237*, 104453. https://doi.org/10.1016/j.gloplacha.2024.104453

Aggarwal, P. K., Romatschke, U., Araguas-Araguas, L., Belachew, D., Longstaffe, F. J., Berg, P., et al. (2016). Proportions of convective and stratiform precipitation revealed in water isotope ratios. *Nature Geoscience*, *9*(8), 624–629. https://doi.org/10.1038/ngeo2739

Arellano, L. N., Beverly, E. J., Selker, J. S., Nelke, M., Singh, G., & Walter, C. (2024). Testing triple oxygen isotope preservation in the new OPEnS totalizer against conventional monthly rainfall collectors. *Chemical Geology*, *668*, 122351. https://doi.org/10.1016/j.chemgeo.2024.122351

Barras, V. J., & Simmonds, I. (2008). Synoptic controls upon δ^{18}O in southern Tasmanian precipitation. *Geophysical Research Letters*, *35*(2), L02804. https://doi.org/10.1029/2007gl031835

Berberan-Santos, M. N., Bodunov, E. N., & Pogliani, L. (1997). On the barometric formula. *American Journal of Physics*, *65*(5), 404–412. https://doi.org/10.1119/1.18555

Berry, G., Reeder, M. J., & Jakob, C. (2011). A global climatology of atmospheric fronts. *Geophysical Research Letters*, *38*(4), L04805. https://doi.org/10.1029/2010gl046451

Borowiak, A., King, A., & Lane, T. (2023). The link between the Madden-Julian Oscillation and rainfall trends in Northwest Australia. *Geophysical Research Letters*, *50*(8), e2022GL101799. https://doi.org/10.1029/2022gl101799

Bureau of Meteorology. (2025). Tropical cyclone reports. Retrieved from http://www.bom.gov.au/cyclone/tropical-cyclone-knowledge-centre/history/past-tropical-cyclones/

Cai, W., Cowan, T., & Thatcher, M. (2012). Rainfall reductions over Southern Hemisphere semi-arid regions: The role of subtropical dry zone expansion. *Scientific Reports*, *2*(1), 702. https://doi.org/10.1038/srep00702

Chang, H. K., Gonçalves, R. D., Aggarwal, P. K., Stradioto, M. R., Hespanhol, E. C., Sturchio, N. C., & Araguas, L. J. (2020). Groundwater isotope ratios reflect convective and stratiform (paleo) precipitation fractions in Brazil. *Journal of Hydrology*, *585*, 124801. https://doi.org/10.1016/j.jhydrol.2020.124801

Charles, S., Fu, G., Silberstein, R., Mpelasoka, F., Mcfarlane, D., Hodgson, G., et al. (2013). Interim report on the hydroclimate of the Pilbara: Past, present and future. *CSIRO Pilbara Water Resource Assessment Report*.

Clark, S., Reeder, M. J., & Jakob, C. (2018). Rainfall regimes over northwestern Australia. *Quarterly Journal of the Royal Meteorological Society*, *144*(711), 458–467. https://doi.org/10.1002/qj.3217

Copernicus Climate Change Service. (2023). ERA5 hourly data on single levels from 1940 to present [Dataset]. *Copernicus Climate Change Service (C3S) Climate Data Store (CDS)*. https://doi.org/10.24381/cds.adbb2d47

Coplen, T. B., De Bièvre, P., Krouse, H. R., Vocke, R. D., Jr., Gröning, M., & Rozanski, K. (1996). Ratios for light-element isotopes standardized for better interlaboratory comparison. *Eos, Transactions American Geophysical Union*, *77*(27), 255. https://doi.org/10.1029/96eo00182

Crawford, J., Azcurra, C. S., Hughes, C. E., Gibson, J. J., & Parkes, S. D. (2019). Comparison of atmospheric water vapour δ^{18}O and δ^{2}H estimated using evaporation pan, rainfall equilibrium and continuous measurements. *Journal of Hydrology*, *576*, 551–560. https://doi.org/10.1016/j.jhydrol.2019.06.056

Crawford, J., Hollins, S. E., Meredith, K. T., & Hughes, C. E. (2017). Precipitation stable isotope variability and subcloud evaporation processes in a semi-arid region. *Hydrological Processes*, *31*(1), 20–34. https://doi.org/10.1002/hyp.10885

Crawford, J., Hughes, C. E., & Chambers, S. D. (2023). Controls on the stable isotope composition of daily precipitation in Sydney Australia: 9 years of daily data, including Radon-222. *Journal of Hydrology*, *617*, 129123. https://doi.org/10.1016/j.jhydrol.2023.129123

Crawford, J., Hughes, C. E., & Parkes, S. D. (2013). Is the isotopic composition of event based precipitation driven by moisture source or synoptic scale weather in the Sydney Basin, Australia? *Journal of Hydrology*, *507*, 213–226. https://doi.org/10.1016/j.jhydrol.2013.10.031

Dansgaard, W. (1964). Stable isotopes in precipitation. *Tellus*, *16*(4), 436–468. https://doi.org/10.1111/j.2153-3490.1964.tb00181.x

Debeire, K., Bock, L., Nowack, P., Runge, J., & Eyring, V. (2025). Constraining uncertainty in projected precipitation over land with causal discovery. *Earth System Dynamics*, *16*(2), 607–630. https://doi.org/10.5194/esd-16-607-2025

Deshpande, R. D., Maurya, A. S., Kumar, B., Sarkar, A., & Gupta, S. K. (2010). Rain-vapor interaction and vapor source identification using stable isotopes from semiarid western India. *Journal of Geophysical Research*, *115*(D23). https://doi.org/10.1029/2010jd014458

Dey, R., Gallant, A. J., & Lewis, S. C. (2020). Evidence of a continent-wide shift of episodic rainfall in Australia. *Weather and Climate Extremes*, *29*, 100274. https://doi.org/10.1016/j.wace.2020.100274

Dogramaci, S., Skrzypek, G., Dodson, W., & Grierson, P. F. (2012). Stable isotope and hydrochemical evolution of groundwater in the semi-arid Hamersley Basin of subtropical northwest Australia. *Journal of Hydrology*, *475*, 281–293. https://doi.org/10.1016/j.jhydrol.2012.10.004

Fierro, A. O., & Leslie, L. M. (2014). Relationships between southeast Australian temperature anomalies and large-scale climate drivers. *Journal of Climate*, *27*(4), 1395–1412. https://doi.org/10.1175/jcli-d-13-00229.1

Froehlich, K., Kralik, M., Papesch, W., Rank, D., Scheifinger, H., & Stichler, W. (2008). Deuterium excess in precipitation of Alpine regions–moisture recycling. *Isotopes in Environmental and Health Studies*, *44*(1), 61–70. https://doi.org/10.1080/10256010801887208

Griffiths, A. D., Treble, P. C., Hope, P., & Rudeva, I. (2022). Rainfall stable water isotope variability in coastal southwestern Western Australia and its relationship to climate on multiple timescales. *Journal of Geophysical Research: Atmospheres*, *127*(1), e2021JD035433. https://doi.org/10.1029/2021jd035433

Gröning, M., Lutz, H. O., Roller-Lutz, Z., Kralik, M., Gourcy, L., & Pöltenstein, L. (2012). A simple rain collector preventing water re-evaporation dedicated for δ^{18}O and δ^{2}H analysis of cumulative precipitation samples. *Journal of Hydrology*, *448*, 195–200. https://doi.org/10.1016/j.jhydrol.2012.04.041

Guan, H., Zhang, X., Skrzypek, G., Sun, Z., & Xu, X. (2013). Deuterium excess variations of rainfall events in a coastal area of South Australia and its relationship with synoptic weather systems and atmospheric moisture sources. *Journal of Geophysical Research: Atmospheres*, *118*(2), 1123–1138. https://doi.org/10.1002/jgrd.50137

Harrington, G. A., Cook, P. G., & Herczeg, A. L. (2002). Spatial and temporal variability of ground water recharge in central Australia: A tracer approach. *Groundwater Series*, *40*(5), 518–527. https://doi.org/10.1111/j.1745-6584.2002.tb02536.x

Hersbach, H., Bell, B., Berrisford, P., Biavati, G., Horányi, A., Muñoz Sabater, J., et al. (2023). ERA5 hourly data on pressure levels from 1940 to present. *Copernicus Climate Change Service (C3S) Climate Data Store (CDS)*. https://doi.org/10.24381/cds.bd0915c6

Holgate, C. M., Van Dijk, A. I. J. M., Evans, J. P., & Pitman, A. J. (2020). Local and remote drivers of southeast Australian drought. *Geophysical Research Letters*, *47*(18), e2020GL090238. https://doi.org/10.1029/2020gl090238

Hollins, S. E., Hughes, C. E., Crawford, J., Cendón, D. I., & Meredith, K. T. (2018). Rainfall isotope variations over the Australian continent–implications for hydrology and isoscape applications. *Science of the Total Environment*, *645*, 630–645. https://doi.org/10.1016/j.scitotenv.2018.07.082

Horita, J., & Wesolowski, D. J. (1994). Liquid-vapor fractionation of oxygen and hydrogen isotopes of water from the freezing to the critical temperature. *Geochimica et Cosmochimica Acta*, *58*(16), 3425–3437. https://doi.org/10.1016/0016-7037(94)90096-5

Hu, J., Emile-Geay, J., Nusbaumer, J., & Noone, D. (2018). Impact of convective activity on precipitation δ^{18}O in isotope-enabled general circulation models. *Journal of Geophysical Research: Atmospheres*, *123*(23), 12–595. https://doi.org/10.1029/2018jd029187

Huang, J., Li, Y., Fu, C., Chen, F., Fu, Q., Dai, A., et al. (2017). Dryland climate change: Recent progress and challenges. *Reviews of Geophysics*, *55*(3), 719–778. https://doi.org/10.1002/2016rg000550

Hughes, C. E., & Crawford, J. (2012). A new precipitation weighted method for determining the meteoric water line for hydrological applications demonstrated using Australian and global GNIP data. *Journal of Hydrology*, *464*, 344–351. https://doi.org/10.1016/j.jhydrol.2012.07.029

Hughes, C. E., & Crawford, J. (2013). Spatial and temporal variation in precipitation isotopes in the Sydney Basin, Australia. *Journal of Hydrology*, *489*, 42–55. https://doi.org/10.1016/j.jhydrol.2013.02.036

Jeffrey, S. J., Carter, J. O., Moodie, K. B., & Beswick, A. R. (2001). Using spatial interpolation to construct a comprehensive archive of Australian climate data. *Environmental Modelling & Software*, *16*(4), 309–330. https://doi.org/10.1016/s1364-8152(01)00008-1

Kaseke, K. F., Wang, L., Wanke, H., Tian, C., Lanning, M., & Jiao, W. (2018). Precipitation origins and key drivers of precipitation isotope (^{18}O, ^{2}H, and ^{17}O) compositions over Windhoek. *Journal of Geophysical Research: Atmospheres*, *123*(14), 7311–7330. https://doi.org/10.1029/2018jd028470

Landshuter, N., Aemisegger, F., & Mölg, T. (2024). Stable water isotope signals and their relation to stratiform and convective precipitation in the tropical Andes. *Journal of Geophysical Research: Atmospheres*, *129*(14), e2023JD040630. https://doi.org/10.1029/2023jd040630

Lekshmy, P. R., Midhun, M., & Ramesh, R. (2018). Influence of stratiform clouds on δD and δ^{18}O of monsoon water vapour and rain at two tropical coastal stations. *Journal of Hydrology*, *563*, 354–362. https://doi.org/10.1016/j.jhydrol.2018.06.001

Lian, X., Piao, S., Chen, A., Huntingford, C., Fu, B., Li, L. Z. X., et al. (2021). Multifaceted characteristics of dryland aridity changes in a warming world. *Nature Reviews Earth & Environment*, *2*(4), 232–250. https://doi.org/10.1038/s43017-021-00144-0

McFarlane, D., Hodgson, G., Commander, P., Barron, O., Silberstein, R., & Aryal, S. (2015). Chapter 2: Overview of the Pilbara. In D. McFarlane (Ed.), *Pilbara water resource assessment* (p. 222). CSIRO Land and Water.

Michelsen, N., van Geldern, R., Roßmann, Y., Bauer, I., Schulz, S., Barth, J. A., & Schüth, C. (2018). Comparison of precipitation collectors used in isotope hydrology. *Chemical Geology*, *488*, 171–179. https://doi.org/10.1016/j.chemgeo.2018.04.032

Misumi, R., Uji, Y., & Maesaka, T. (2021). Modification of raindrop size distribution due to seeder–feeder interactions between stratiform precipitation and shallow convection observed by X-band polarimetric radar and optical disdrometer. *Atmospheric Science Letters*, *22*(7), e1034. https://doi.org/10.1002/asl.1034

Munksgaard, N. C., Zwart, C., Haig, J., Cernusak, L. A., & Bird, M. I. (2020). Coupled rainfall and water vapour stable isotope time series reveal tropical atmospheric processes on multiple timescales. *Hydrological Processes*, *34*(1), 111–124. https://doi.org/10.1002/hyp.13576

Natali, S., Nigro, M., Baneschi, I., Giannecchini, R., Doveri, M., & Zanchetta, G. (2024). On the reliability of tube-dip-in-water precipitation collectors in isotope hydrology: A field experiment for low rainfall amounts. *Journal of Hydrology*, *644*, 132096. https://doi.org/10.1016/j.jhydrol.2024.132096

Noone, D. (2012). Pairing measurements of the water vapor isotope ratio with humidity to deduce atmospheric moistening and dehydration in the tropical midtroposphere. *Journal of Climatology*, *25*(13), 4476–4494. https://doi.org/10.1175/jcli-d-11-00582.1

O'Donnell, A. J., Cook, E. R., Palmer, J. G., Turney, C. S., Page, G. F., & Grierson, P. F. (2015). Tree rings show recent high summer-autumn precipitation in northwest Australia is unprecedented within the last two centuries. *PLoS One*, *10*(6), e0128533. https://doi.org/10.1371/journal.pone.0128533

Parameswaran, K., & Murthy, B. K. (1990). Altitude profiles of tropospheric water vapor at low latitudes. *Journal of Applied Meteorology and Climatology*, *29*(8), 665–679. https://doi.org/10.1175/1520-0450(1990)029<0665:apotwv>2.0.co;2

Prein, A. F., Ge, M., Valle, A. R., Wang, D., & Giangrande, S. E. (2022). Towards a unified setup to simulate mid-latitude and tropical mesoscale convective systems at kilometer-scales. *Earth and Space Science*, *9*(8), e2022EA002295. https://doi.org/10.1029/2022ea002295

R Core Team. (2021). *R: A language and environment for statistical computing*. R Foundation for Statistical Computing. Retrieved from https://www.R-project.org/

Reverdin, G., Waelbroeck, C., Pierre, C., Akhoudas, C., Aloisi, G., Benetti, M., et al. (2022). The CISE-LOCEAN seawater isotopic database (1998–2021). *Earth System Science Data*, *14*(6), 2721–2735. https://doi.org/10.5194/essd-14-2721-2022

Rojas, R., Commander, P., McFarlane, D., Ali, R., Dawes, W., Barron, O., & Charles, S. (2018). Groundwater resource assessment and conceptualization in the Pilbara Region, Western Australia. *Earth Systems and Environment*, *2*(2), 345–365. https://doi.org/10.1007/s41748-018-0051-0

Rouillard, A., Skrzypek, G., Dogramaci, S., Turney, C., & Grierson, P. F. (2015). Impacts of high inter-annual variability of rainfall on a century of extreme hydrologic regime of northwest Australia. *Hydrology and Earth System Sciences*, *19*(4), 2057–2078. https://doi.org/10.5194/hess-19-2057-2015

Rozanski, K., Araguas-Araguas, L., & Gonfiantini, R. (1992). Relation between long-term trends of oxygen-18 isotope composition of precipitation and climate. *Science*, *258*(5084), 981–985. https://doi.org/10.1126/science.258.5084.981

Salamalikis, V., Argiriou, A. A., & Dotsika, E. (2016). Isotopic modeling of the sub-cloud evaporation effect in precipitation. *Science of the Total Environment*, *544*, 1059–1072. https://doi.org/10.1016/j.scitotenv.2015.11.072

Schumacher, C., & Houze, R. A., Jr. (2003). Stratiform rain in the tropics as seen by the TRMM precipitation radar. *Journal of Climate*, *16*(11), 1739–1756. https://doi.org/10.1175/1520-0442(2003)016<1739:sritta>2.0.co;2

Sekizawa, S., Nakamura, H., & Kosaka, Y. (2018). Interannual variability of the Australian summer monsoon system internally sustained through wind-evaporation feedback. *Geophysical Research Letters*, *45*(15), 7748–7755. https://doi.org/10.1029/2018gl078536

Sharmila, S., & Hendon, H. H. (2020). Mechanisms of multiyear variations of Northern Australia wet-season rainfall. *Scientific Reports*, *10*(1), 5086. https://doi.org/10.1038/s41598-020-61482-5

Shi, G., Cai, W., Cowan, T., Ribbe, J., Rotstayn, L., & Dix, M. (2008). Variability and trend of North West Australia rainfall: Observations and coupled climate modeling. *Journal of Climate*, *21*(12), 2938–2959. https://doi.org/10.1175/2007jcli1908.1

Sinha, N., & Chakraborty, S. (2020). Isotopic interaction and source moisture control on the isotopic composition of rainfall over the Bay of Bengal. *Atmospheric Research*, *235*, 104760. https://doi.org/10.1016/j.atmosres.2019.104760

Skrzypek, G. (2013). Normalization procedures and reference material selection in stable HCNOS isotope analyses: An overview. *Analytical and Bioanalytical Chemistry*, *405*(9), 2815–2823. https://doi.org/10.1007/s00216-012-6517-2

Skrzypek, G., Dogramaci, S., Page, G. F., Rouillard, A., & Grierson, P. F. (2019). Unique stable isotope signatures of large cyclonic events as a tracer of soil moisture dynamics in the semiarid subtropics. *Journal of Hydrology*, *578*, 124124. https://doi.org/10.1016/j.jhydrol.2019.124124

Skrzypek, G., & Ford, D. (2014). Stable isotope analysis of saline water samples on a cavity ring-down spectroscopy instrument. *Environmental Science & Technology*, *48*(5), 2827–2834. https://doi.org/10.1021/es4049412

Skrzypek, G., Siller, A., McCallum, J. L., & Dogramaci, S. (2023). Groundwater recharge through internally drained basins in a semiarid climate, Western Australia. *Journal of Hydrology: Regional Studies*, *47*, 101388. https://doi.org/10.1016/j.ejrh.2023.101388

Sodemann, H., Schwierz, C., & Wernli, H. (2008). Interannual variability of Greenland winter precipitation sources: Lagrangian moisture diagnostic and North Atlantic Oscillation influence. *Journal of Geophysical Research*, *113*(D3), D03106. https://doi.org/10.1029/2007jd008503

Stein, A. F., Draxler, R. R., Rolph, G. D., Stunder, B. J. B., Cohen, M. D., & Ngan, F. (2015). NOAA's HYSPLIT atmospheric transport and dispersion modeling system. *Bulletin of the American Meteorological Society*, *96*(12), 2059–2077. https://doi.org/10.1175/bams-d-14-00110.1

Stewart, M. K. (1975). Stable isotope fractionation due to evaporation and isotopic exchange of falling waterdrops: Applications to atmospheric processes and evaporation of lakes. *Journal of Geophysical Research*, *80*(9), 1133–1146. https://doi.org/10.1029/JC080i009p01133

Sun, C., Tian, L., Shanahan, T. M., Partin, J. W., Gao, Y., Piatrunia, N., & Banner, J. (2022). Isotopic variability in tropical cyclone precipitation is controlled by Rayleigh distillation and cloud microphysics. *Communications Earth & Environment*, *3*(1), 50. https://doi.org/10.1038/s43247-022-00381-1

Tugwell-Wootton, T., Skrzypek, G., Dogramaci, S., McCallum, J., & Grierson, P. F. (2020). Soil moisture evaporative losses in response to wet-dry cycles in a semiarid climate. *Journal of Hydrology*, *590*, 125533. https://doi.org/10.1016/j.jhydrol.2020.125533

Wan, C., Dogramaci, S., Gleeson, J., Hedley, P., Grierson, P., Gibson, J., & Skrzypek, G. (2026). Stable isotope record of precipitation dynamics in the semi-arid subtropics [Dataset]. *Figshare*. https://doi.org/10.6084/m9.figshare.31517590

Wang, S., Shi, Y., Xing, M., Wu, H., Pang, H., Lei, S., et al. (2024). Quantifying the below-cloud evaporation of raindrops using near-surface water vapour isotopes: Applications in humid and arid climates in East Asia. *Journal of Hydrology*, *638*, 131561. https://doi.org/10.1016/j.jhydrol.2024.131561

Wang, S., Zhang, M., Hughes, C. E., Crawford, J., Wang, G., Chen, F., et al. (2018). Meteoric water lines in arid Central Asia using event-based and monthly data. *Journal of Hydrology*, *562*, 435–445. https://doi.org/10.1016/j.jhydrol.2018.05.034

Wierik, S. A., Cammeraat, E. L., Gupta, J., & Artzy-Randrup, Y. A. (2021). Reviewing the impact of land use and land-use change on moisture recycling and precipitation patterns. *Water Resources Research*, *57*(7), e2020WR029234. https://doi.org/10.1029/2020WR029234

Worden, J., Noone, D., & Bowman, K. (2007). Importance of rain evaporation and continental convection in the tropical water cycle. *Nature*, *445*(7127), 528–532. https://doi.org/10.1038/nature05508

Xia, Y., Huang, Q., Yao, S., & Sun, T. (2021). Multiscale causes of persistent heavy rainfall in the Meiyu period over the middle and lower reaches of the Yangtze River. *Frontiers in Earth Science*, *9*, 700878. https://doi.org/10.3389/feart.2021.700878

Xu, S., Gentine, P., Li, L., Wang, L., Yu, Z., Dong, N., et al. (2023). Response of ecosystem productivity to high vapor pressure deficit and low soil moisture: Lessons learned from the global eddy-covariance observations. *Earth's Future*, *11*(8), e2022EF003252. https://doi.org/10.1029/2022ef003252

Xu, X., Zhao, Z., & Skrzypek, G. (2025). Stable isotope disequilibrium between soil bound water and soil bulk water–implications for estimations of plant water sources. *Journal of Hydrology*, *650*, 132544. https://doi.org/10.1016/j.jhydrol.2024.132544

Yang, S., & Smith, E. A. (2008). Convective–stratiform precipitation variability at seasonal scale from 8 yr of TRMM observations: Implications for multiple modes of diurnal variability. *Journal of Climate*, *21*(16), 4087–4114. https://doi.org/10.1175/2008jcli2096.1

Yao, T., Zhang, X., Guan, H., Zhou, H., Hua, M., & Wang, X. (2018). Climatic and environmental controls on stable isotopes in atmospheric water vapor near the surface observed in Changsha, China. *Atmospheric Environment*, *189*, 252–263. https://doi.org/10.1016/j.atmosenv.2018.07.008

Yoshimura, K., Kanamitsu, M., Noone, D., & Oki, T. (2008). Historical isotope simulation using reanalysis atmospheric data. *Journal of Geophysical Research*, *113*(D19), D19108. https://doi.org/10.1029/2008jd010074

Yu, W., Guo, R., Thompson, L. G., Zhang, J., Lewis, S., Jing, Z., et al. (2024). Water isotope ratios reflect convection intensity rather than rain type proportions in the pantropics. *Science Advances*, *10*(33), eado3258. https://doi.org/10.1126/sciadv.ado3258

Zhu, G., Zhang, Z., Guo, H., Zhang, Y., Yong, L., Wan, Q., et al. (2021). Below-cloud evaporation of precipitation isotopes over mountains, oases, and deserts in arid areas. *Journal of Hydrometeorology*, *22*(10), 2533–2545. https://doi.org/10.1175/jhm-d-20-0170.1

Zwart, C., Munksgaard, N. C., Kurita, N., & Bird, M. I. (2016). Stable isotopic signature of Australian monsoon controlled by regional convection. *Quaternary Science Reviews*, *151*, 228–235. https://doi.org/10.1016/j.quascirev.2016.09.010

Zwart, C., Munksgaard, N. C., Protat, A., Kurita, N., Lambrinidis, D., & Bird, M. I. (2018). The isotopic signature of monsoon conditions, cloud modes, and rainfall type. *Hydrological Processes*, *32*(15), 2296–2303. https://doi.org/10.1002/hyp.13140